



Article

Solar Light-Assisted Oxidative Degradation of Ciprofloxacin in Aqueous Solution by Iron(III) Chelated Cross-Linked Chitosan Immobilized on a Glass Plate

Soma Saha¹, Tapan Kumar Saha^{1,*}, Subarna Karmaker¹, Zinia Islam², Serhiy Demeshko³, Holm Frauendorf⁴ and Franc Meyer^{3,*}

¹ Department of Chemistry, Jahangirnagar University, Savar 1342, Bangladesh; somasaha200048@gmail.com (S.S.); ksubarna_ju@yahoo.com (S.K.)

² Department of Biotechnology and Genetic Engineering, Jahangirnagar University, Savar 1342, Bangladesh; zinia025@gmail.com

³ Institute of Inorganic Chemistry, University of Göttingen, Tammannstrasse 4, D-37077 Göttingen, Germany; sdemesco@gwdg.de

⁴ Institute of Organic and Biomolecular Chemistry, University of Göttingen, Tammannstrasse 2, D-37077 Göttingen, Germany; holm.frauendorf@chemie.uni-goettingen.de

* Correspondence: tksaha_ju@yahoo.com (T.K.S.); franc.meyer@chemie.uni-goettingen.de (F.M.)

Abstract: The massive worldwide use of antibiotics leads to water pollution and increasing microbial resistance. Hence, the removal of antibiotic residues is a key issue in water remediation. Here, we report the solar light-assisted oxidative degradation of ciprofloxacin (CPF), using H₂O₂ in aqueous solution, catalyzed by iron(III) chelated cross-linked chitosan (Fe^{III}-CS-GLA) immobilized on a glass plate. The Fe^{III}-CS-GLA catalyst was characterized by FTIR and ⁵⁷Fe-Mössbauer spectroscopies as well as X-ray diffraction, revealing key structural motifs and a high-spin ferric character of the metal. Catalytic degradation of CPF was investigated as a function of solar light irradiation time, solution pH, concentration of H₂O₂ and CPF, as well as cross-linker dosage and iron(III) content in Fe^{III}-CS-GLA. The system was found to serve as an efficient catalyst with maximum CPF degradation at pH 3. The specific ·OH scavenger mannitol significantly reduces the degradation rate, indicating that hydroxyl radicals play a key role. The mechanism of catalytic CPF degradation was evaluated in terms of pseudo-first-order and Langmuir-Hinshelwood kinetic models; adsorption of CPF onto the Fe^{III}-CS-GLA surface was evidenced by field emission scanning electron microscopy coupled with energy dispersive X-ray spectroscopy. Fe^{III}-CS-GLA can be reused multiple times with only minor loss of catalytic efficiency. Antimicrobial activity tests performed against both Gram-negative (*Escherichia coli* DH5 α , *Salmonella typhi* AF4500) and Gram-positive bacteria (*Bacillus subtilis* RBW) before and after treatment confirmed complete degradation of CPF. These results establish the immobilized Fe^{III}-CS-GLA as a rugged catalyst system for efficient photo-Fenton type degradation of antibiotics in aqueous solutions.

Keywords: ciprofloxacin; oxidative degradation; water treatment; kinetic studies; antimicrobial activity



Citation: Saha, S.; Saha, T.K.; Karmaker, S.; Islam, Z.; Demeshko, S.; Frauendorf, H.; Meyer, F. Solar Light-Assisted Oxidative Degradation of Ciprofloxacin in Aqueous Solution by Iron(III) Chelated Cross-Linked Chitosan Immobilized on a Glass Plate. *Catalysts* **2022**, *12*, 475. <https://doi.org/10.3390/catal12050475>

Academic Editor: Antonio Eduardo Palomares

Received: 22 February 2022

Accepted: 12 April 2022

Published: 23 April 2022

Publisher's Note: MDPI stays neutral with regard to jurisdictional claims in published maps and institutional affiliations.



Copyright: © 2022 by the authors. Licensee MDPI, Basel, Switzerland. This article is an open access article distributed under the terms and conditions of the Creative Commons Attribution (CC BY) license (<https://creativecommons.org/licenses/by/4.0/>).

1. Introduction

Antibiotics are used to treat microbial infections but it is well documented that the excess use of antibiotics leads to water pollution and antibiotic resistant microorganisms, which translates into higher medical costs, prolonged hospital stays, and increased mortality [1–3]. The reasons behind the high level of antibiotic residues in wastewater are the widespread use of pharmaceuticals around the world, including animal farms, agricultural land, hospital wastes etc. [4–10]. Several methods such as adsorption [11,12], advanced oxidation processes [13], sonochemistry [14], ionizing radiation [15], photodegradation [16], ozonation [17], ultraviolet irradiation [18], reverse osmosis [19], and coagulation [20], have been proposed to remove antibiotics from aqueous wastewater. Adsorption is found to be

one of the most common and easiest methods in this context, but the removal process is very slow and the efficiency is low. Therefore, researchers are seeking alternative ways of removing antibiotics from wastewater [21,22].

In this study, one of the most commonly used antibiotics, ciprofloxacin hydrochloride (CPF) (Figure 1a), was considered as an exemplary substrate. CPF is a member of the broad-spectrum fluoroquinolones (FQs), which actively work against both Gram-positive and Gram-negative bacteria, and it is used worldwide for the treatment of bacterial infections in humans and animals [23,24]. The presence of this broad-spectrum antibiotic in aquatic systems may cause serious threats to the ecosystem and human health by inducing proliferation of bacterial drug resistance [25]. CPF is not biodegradable and is a highly recalcitrant pollutant, and even minute amounts of this antibiotic are problematic. Moreover, several reports confirmed the presence of CPF residues in fish tissues, which can have serious consequences for human health [26,27]. Thus, the removal of CPF from aquatic environments has already become a matter of concern. Various studies have addressed the removal of CPF from aqueous solutions by adsorption [28], membrane filtration [29], ultraviolet-activated persulfate [30], electrochemically activated persulfate [31,32], sonolysis [33], heterogeneous catalytic ozonation [34], advanced oxidation processes [35], pillared iron catalyst [36] Fenton's oxidation [37], photo-Fenton degradation [38], FeS₂/SiO₂ microspheres [39], photodegradation [40], and photocatalytic processes using ZnO nanoparticles [41], graphene oxide-BiVO₄ composites [42], titanium dioxide (TiO₂) [43,44], silver/iron oxide/zinc oxide heterostructures [45], etc. Here we report the use of iron(III) chelated cross-linked chitosan, Fe^{III}-CS-GLA, in the presence of hydrogen peroxide and solar light as a novel approach for the elimination of CPF from aqueous solutions. Lee and Lee previously investigated oxidative degradation of trichloroethylene in water by using Fe^{II} chelated with cross-linked chitosan [46], and Neto et al. [47] evaluated the removal of As^{III} and As^V by employing crosslinked chitosan-Fe^{III} (Ch-FeCL) beads as an adsorbent.

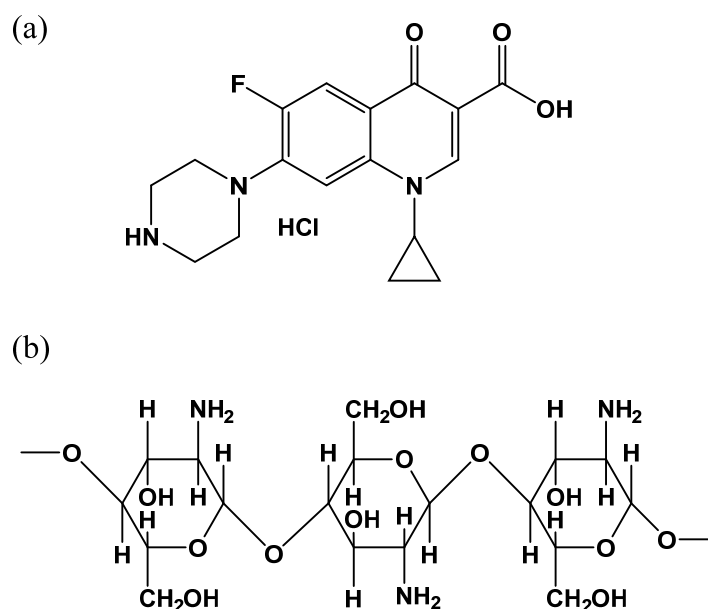


Figure 1. Structures of (a) CPF and (b) CS.

In the present study, the solar light-assisted oxidative degradation of CPF mediated by hydrogen peroxide and Fe^{III}-CS-GLA immobilized on a glass plate was investigated in aqueous solutions under various pH conditions. Chitosan (CS) is a linear polysaccharide composed of randomly distributed β -(1-4)-linked *D*-glucosamine (deacetylated unit) and *N*-acetyl-*D*-glucosamine (acetylated unit) (Figure 1b). Chitosan has many useful characteristics such as hydrophilicity, biocompatibility, biodegradability and antibacterial properties. It can also selectively bind with various compounds and materials such as cholesterol, fats,

metal ions, proteins, and tumor cells [48]. Chitosan is a cheap and commercially available biodegradable polymer. Thus, the process costs are low, and the present technique can potentially be used for removing antibiotics from aqueous solutions on a large scale.

The objectives of this comprehensive study were (i) to establish and assess robust protocols for preparing Fe^{III}-CS-GLA immobilized on a glass plate by varying the concentration of glutaraldehyde (GLA) and iron(III); (ii) to characterize the Fe^{III}-CS-GLA catalyst using Fourier transform infrared (FTIR) and ⁵⁷Fe Mössbauer spectroscopy as well as X-ray diffraction (XRD); (iii) to perform batch experiments for investigating the effects of various parameters including solar light irradiation time, solution pH, cross-linker GLA and iron(III) dosages in Fe^{III}-CS-GLA, and concentrations of H₂O₂ and CPF on the kinetics of catalytic degradation of CPF, and to examine the effect of a hydroxyl radical scavenger on the catalysis; (iv) to monitor both adsorption and degradation of CPF over Fe^{III}-CS-GLA by performing field emission scanning electron microscopy (FE-SEM) and energy dispersive X-ray (EDX) investigations; (v) to analyze the degradation product of CPF by HPLC-UV-ESI-MS; (vi) to evaluate antimicrobial activities of CPF against both Gram-negative (i.e., *Escherichia coli* DH5 α and *Salmonella typhi* AF450) and Gram-positive (i.e., *Bacillus subtilis* RBW) bacteria before and after catalytic degradation; and (vii) to investigate the reusability of the Fe^{III}-CS-GLA catalyst for the oxidative degradation of CPF in aqueous solutions.

2. Results and Discussion

2.1. Characterization Results

2.1.1. FTIR Spectra

The Fe^{III}-CS-GLA was prepared from CS, FeCl₂·4H₂O and GLA under aerobic conditions, following the method developed by Lee and Lee [46] with slight modifications as detailed in the experimental section. Figure 2 shows the FTIR spectra of CS and Fe^{III}-CS-GLA recorded as KBr pellets in the range of 400–4000 cm⁻¹. In the spectrum of CS (Figure 2a), the broad and intense peak in the region 3292–3361 cm⁻¹ represents N–H and O–H stretching with intramolecular hydrogen bonds. The bands at around 2875 cm⁻¹ with a shoulder at 2921 cm⁻¹ correspond to the asymmetric and symmetric C–H stretching, respectively. The peaks located at 1654, 1597, 1550 and 1321 cm⁻¹ are assigned to the stretching vibration of the C = O bond (amide I), the bending vibration of the N–H bond (primary amine), the bending vibration of the N–H bond (amide II) and the stretching vibration of the C–N bond (amide III), respectively [49]. The CH₂ bending and CH₃ symmetrical deformations were identified by the presence of peaks at around 1422 and 1377 cm⁻¹, respectively. The peak at 1153 cm⁻¹ represents the asymmetric stretching vibration of the C–O–C bridge. The peaks at 1066 and 1028 cm⁻¹ are attributed to C–O stretching vibrations. The characteristic signal for the C–H deformation of the β -glycosidic bond is observed at 898 cm⁻¹.

The spectrum of Fe^{III}-CS-GLA (Figure 2b) is overall similar to the one of pure CS but shows some characteristic changes. Specifically, an additional absorption band is observed at 1660 cm⁻¹ and assigned to the stretching vibration of C = N bonds, indicating the formation of Schiff bases as a result of the reaction between the aldehyde group of GLA and the amino group of CS during the crosslinking process. Furthermore, a sharp band appearing at 619 cm⁻¹ is assigned to Fe–N stretching, reflecting coordination of the metal ion [47,50].

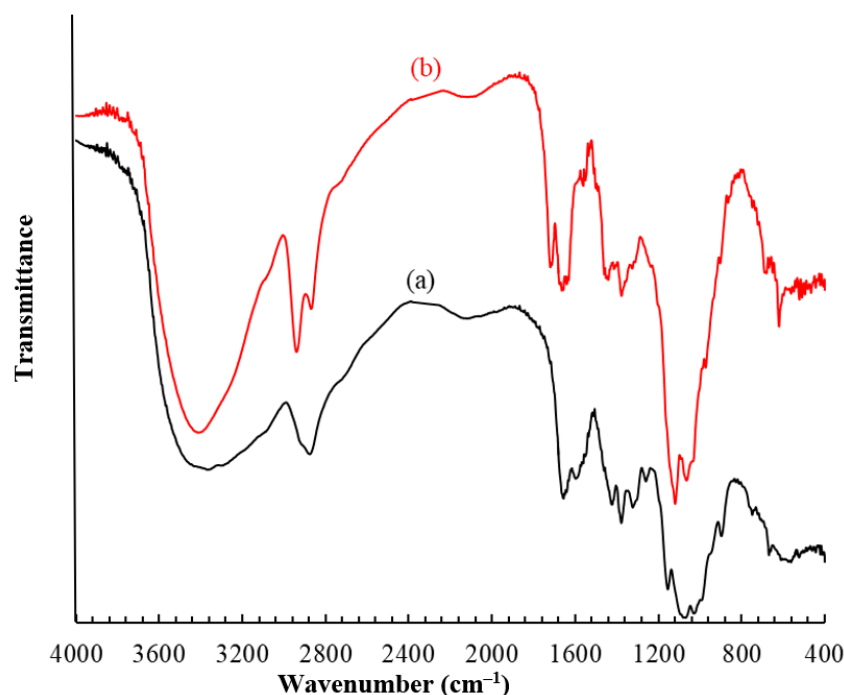


Figure 2. FTIR spectra of pure CS (a) and Fe^{III}-CS-GLA (b). The spectra were recorded as KBr pellets.

2.1.2. Mössbauer Spectroscopy

To determine the oxidation state and to gain insight into the electronic structure of the immobilized iron species in Fe-CS-GLA, ⁵⁷Fe Mössbauer spectroscopy was applied. Various samples of Fe-CS-GLA prepared by varying the initial concentration of iron at constant CS and GLA concentrations were analyzed, as described in the materials and methods section. All Mössbauer spectra were recorded at 80 K, and a typical Mössbauer spectrum of Fe-CS-GLA is shown in Figure 3 (in that case the iron concentration was 7.5 mM). It is noted that all Mössbauer spectra were rather similar, featuring one quadrupole doublet with isomer shift $\delta = 0.48\text{--}0.49$ mm/s and quadrupole splitting $\Delta E_Q = 0.77\text{--}0.79$ mm/s. These values are characteristic of high-spin iron(III) ions [51], as was previously observed in other Fe-chitosan complexes [52,53]. Webster et al. [54] proposed that iron(III) complexed with GLA cross-linked CS has an octahedral coordination sphere composed of two N-donors and two alcohol groups from the opposite glucosamine units in the equatorial plane, with two additional alcohol hydroxyl groups from C-6 in apical positions. The present isomer shift values ($\delta = 0.48\text{--}0.49$ mm/s) and the characteristic Fe–N stretching vibration in the IR spectrum (Figure 2b) are in accordance with the proposed {N₂O₄} ligation of the iron ions in Fe^{III}-CS-GLA.

2.1.3. X-ray Diffraction (XRD)

XRD patterns of pure CS and Fe^{III}-CS-GLA are shown in Figure S1. The XRD pattern of (Figure S1a) CS shows its typical broad peaks for crystalline fragments at 2θ values of 11° for segments with --NH_2 groups and 20° for the hydrophilic pockets in the chitosan, respectively [54]. The former peak disappeared in the XRD pattern of Fe^{III}-CS-GLA and only a broad feature at the $2\theta = 17^\circ$ is present (Figure S1b). These changes upon cross-linking and iron coordination reflect the formation of Schiff bases as a result of the reaction between the GLA and the --NH_2 groups of CS as well as the formation of Fe^{III}-CS-GLA complexes through --NH_2 binding sites and the hydrophilic pockets in the CS [50,54].

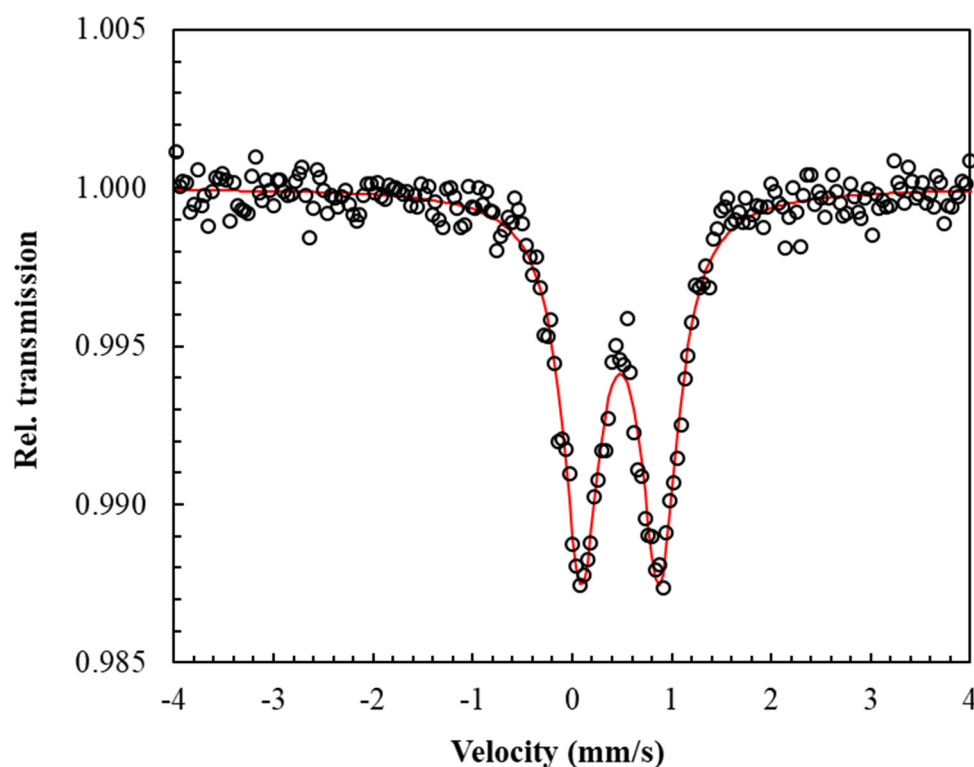


Figure 3. Typical zero-field ^{57}Fe Mössbauer spectrum of Fe^{III} -CS-GLA recorded at 80 K (the iron concentration during preparation was 7.5 mM). The solid line represents the best fit with parameters $\delta = 0.48$ mm/s, $\Delta E_{\text{Q}} = 0.79$ mm/s and line width $\Gamma = 0.46$ mm/s.

2.1.4. Surface Morphology and Elemental Composition of Fe^{III} -CS-GLA

The surface morphology and elemental composition of the synthesized Fe^{III} -CS-GLA immobilized on a glass plate were investigated using field emission scanning electron microscopy (FE-SEM) and energy-dispersive X-ray spectroscopy (EDX) analysis before and after its use for the catalytic degradation of CPF. A smooth surface structure of Fe^{III} -CS-GLA is clearly observed in the FE-SEM image (Figure 4a); the corresponding EDX data are shown in Figure S2a. After CPF degradation, the FE-SEM image of the surface of Fe^{III} -CS-GLA becomes brighter (Figure 4b) and the presence of precipitates suggests that a layer of CPF is present on the surface of Fe^{III} -CS-GLA. A peak for fluorine was not detected in the EDX data of pristine Fe^{III} -CS-GLA (Figure S2a), but it is clearly present in the EDX analysis after using Fe^{III} -CS-GLA in the CPF degradation reaction (Figure S2b). Moreover, the mass percentage of nitrogen and chlorine becomes higher after degradation of CPF (Figure S2b), which indicates that CPF adsorption on the surface of Fe^{III} -CS-GLA takes place under the catalytic conditions. The EDX data also show that the mass percentage of Fe slightly decreases after Fe^{III} -CS-GLA has been used for the CPF degradation reaction, indicative of some leaching of Fe^{III} during the catalytic process in aqueous solution at pH 3 [45].

2.2. Catalysis Results

2.2.1. Effect of Solar Light Irradiation

In order to explore suitable conditions for the catalytic degradation of CPF mediated by Fe^{III} -CS-GLA, H_2O_2 and light, a number of control experiments omitting one or several components such as

- (i) 50 μM CPF + CS-GLA immobilized on a glass plate + solar light;
- (ii) 50 μM CPF + Fe^{III} -CS-GLA immobilized on a glass plate + solar light;
- (iii) 50 μM CPF + Fe^{III} -CS-GLA immobilized on a glass plate + H_2O_2 + dark;
- (iv) 50 μM CPF + Fe^{III} -CS-GLA immobilized on a glass plate + H_2O_2 + solar light

were performed in aqueous solution (pH 3) as described in the materials and methods section. The reaction progress was assessed by UV-vis spectroscopic monitoring of the characteristic absorption peak of CPF at 276 nm [32]. It is noted that the UV-vis spectra remained nearly constant in aqueous solution (pH 3) over 180 min for the control experiments (i), (ii) and (iii), indicating that CPF is not degraded under those conditions. Indeed, the spectrophotometric data confirm that the presence of both solar light and H₂O₂ is required for achieving Fe^{III}-CS-GLA catalyzed oxidative degradation of CPF in water. The typical time-resolved spectral changes during oxidative degradation of CPF in experiment (iv) are depicted in Figure 5, evidencing that the characteristic absorption peak of CPF at 276 nm gradually decreases with time and completely disappears within 180 min.

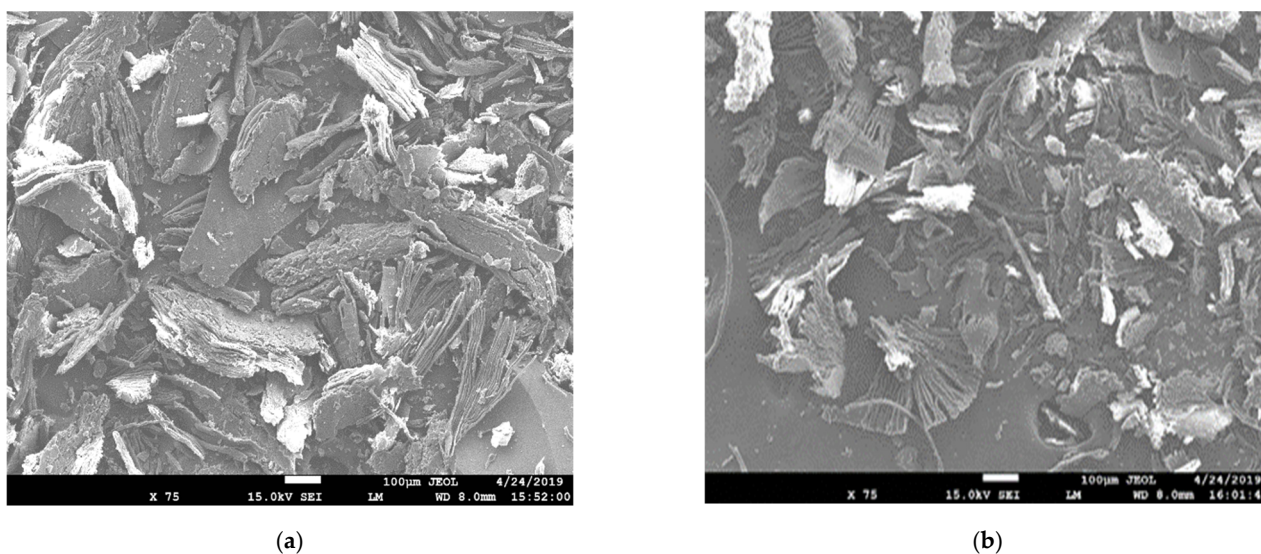


Figure 4. FE-SEM photograph of Fe^{III}-CS-GLA before (a) and after (b) its use in the catalytic degradation of CPF.

Changes in absorbance of the characteristic peak (λ_{\max} : 276 nm) with time are depicted in Figure 6 for the various control experiments. The kinetic trace of CPF degradation in experiment (iv) follows a single exponential decay with time (Figure 6a), which was then used to determine a pseudo-first-order rate constant (k_{obs}) for the solar light-assisted oxidative degradation of CPF catalyzed by Fe^{III}-CS-GLA/H₂O₂. A typical pseudo-first-order kinetic plot $\ln A_t$ vs. t is shown in Figure 6b. The value of the observed rate constant (k_{obs} : 0.0134 min⁻¹; Table 1) was determined from the slope of the straight line, and the half-life time was estimated to be 51.7 min. Similar reaction kinetics (k_{obs} : 0.0117 min⁻¹) were reported for the photocatalytic degradation of ciprofloxacin using ZnO nanoparticles in aqueous solution (pH 4) [41]. Other research groups also investigated the oxidative degradation of CPF by using sonolysis and various catalysts in aqueous solution; the reported k_{obs} values were 0.0210 min⁻¹ for the sonolysis process at pH 3 [33], 0.0253 min⁻¹ for CPF degradation using a pillared iron catalyst (Fe-Lap-RD) at pH 3 [36], 0.0210 min⁻¹ using TiO₂ at pH 3 [43], and 0.0051 min⁻¹ for Ag/Fe₂O₃/ZnO heterostructures at pH 4 [45], respectively (Table 1).

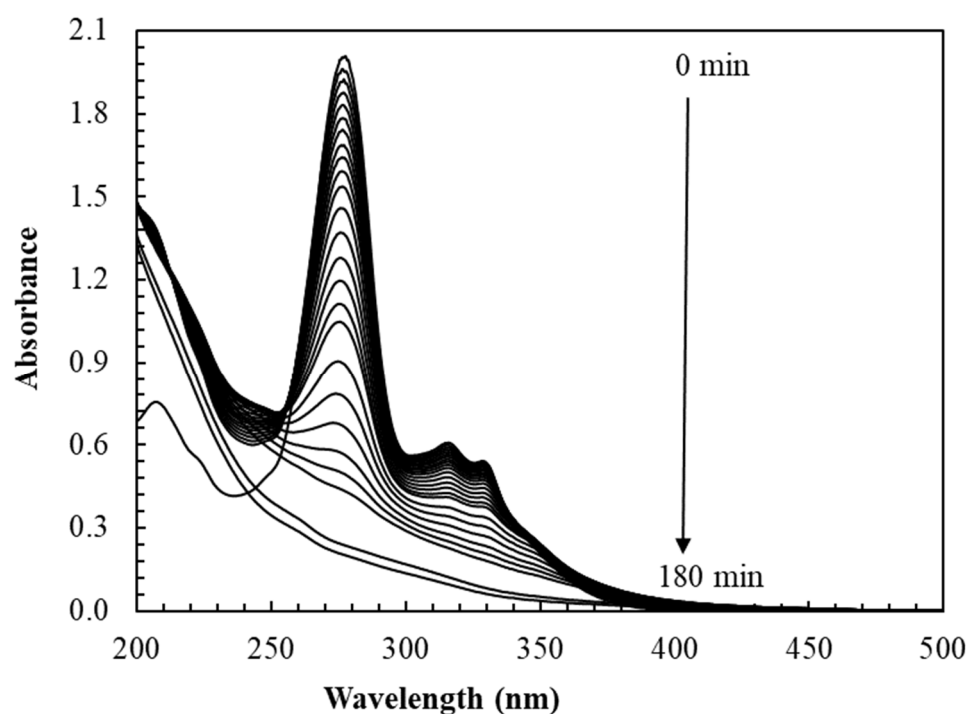


Figure 5. Typical time-resolved spectral changes observed in solar light-assisted oxidative degradation of CPF catalyzed by Fe^{III}-CS-GLA in aqueous solution. Experimental conditions: [CPF]₀: 50 μM; [Fe^{III}]₀ in Fe^{III}-CS-GLA: 1.25 mM; [GLA]₀ in Fe^{III}-CS-GLA: 90 mM; [H₂O₂]₀: 6 mM; volume of CPF solution: 250 mL; pH: 3; light intensity: 70,000–90,000 Lux; solar light irradiation time: 180 min.

Table 1. Pseudo-first order rate constants (k_{obs}) of CPF degradation by different processes.

Degradation Process	pH	k_{obs} (min ⁻¹)	References
Sonolysis	3	0.0210	[33]
Pillared iron catalyst (Fe-Lap-RD)	3	0.0253	[36]
ZnO nanoparticles	4	0.0117	[41]
Commercial anatase TiO ₂	3	0.0210	[43]
Ag/Fe ₂ O ₃ /ZnO heterostructures	4	0.0051	[45]
Fe ^{III} -CS-GLA/H ₂ O ₂	3	0.0134	This work

2.2.2. Effect of pH

The solution pH is an important control parameter for the CPF degradation process. The solar light-assisted oxidative degradation of CPF catalyzed by Fe^{III}-CS-GLA immobilized on a glass plate in aqueous solution in the range pH 2–12 at fixed initial concentration of CPF (50 μM) and H₂O₂ (6 mM) was investigated for 180 min. The effects of pH on k_{obs} and CPF removal efficiency are shown in Figure 7. Starting at pH 2 and gradually increasing the pH, the values of k_{obs} and CPF removal efficiency significantly increase to reach their maximum values at pH 3 (k_{obs} : 0.0134 min⁻¹ and CPF removal efficiency: 90.25%), but then decrease upon raising the pH up to pH ≤ 5.5 (k_{obs} : 0.0038 min⁻¹ and CPF removal efficiency: 44.8%). Further increase of pH leads to variations that peak at pH 7 for CPF removal efficiency (k_{obs} : 0.0047 min⁻¹ and CPF removal efficiency: 63.0%) and for both parameters at pH 10.5 (k_{obs} : 0.0079 min⁻¹ and CPF removal efficiency: 63.8%). Both k_{obs} and CPF removal efficiency dramatically drop at pH ≥ 11. The pH dependence can likely be explained by the stability of hydroxyl radicals ([•]OH) and the degree of protonation of CPF molecules depending on the solution pH. CPF exists as CPF³⁺ at pH < 3.64, CPF²⁺ at pH ≤ 5.05, CPF⁺ at pH ≤ 6.95, CPF at pH 6.95 to 8.95 and CPF⁻ at pH > 8.95 [33]. Bel et al. reported a similar correlation between the pseudo-first-order degradation rate constants and solution pH for the sonolysis of ciprofloxacin [33]. It has also been reported that the best photo-assisted degradation of CPF catalyzed by a modified laponite clay-based iron(III)

nanocomposite (Fe-Lap-RD: 1 g/L) in the presence of H_2O_2 (60 mM) occurs in aqueous solution at pH 3 [36]. The present results are in accordance with those earlier observations. Thus, the solar light-assisted oxidative degradation of CPF catalyzed by Fe^{III} -CS-GLA immobilized on a glass plate is most efficient in aqueous solution at pH 3 and hence, all further experiments were carried out at solution pH 3.

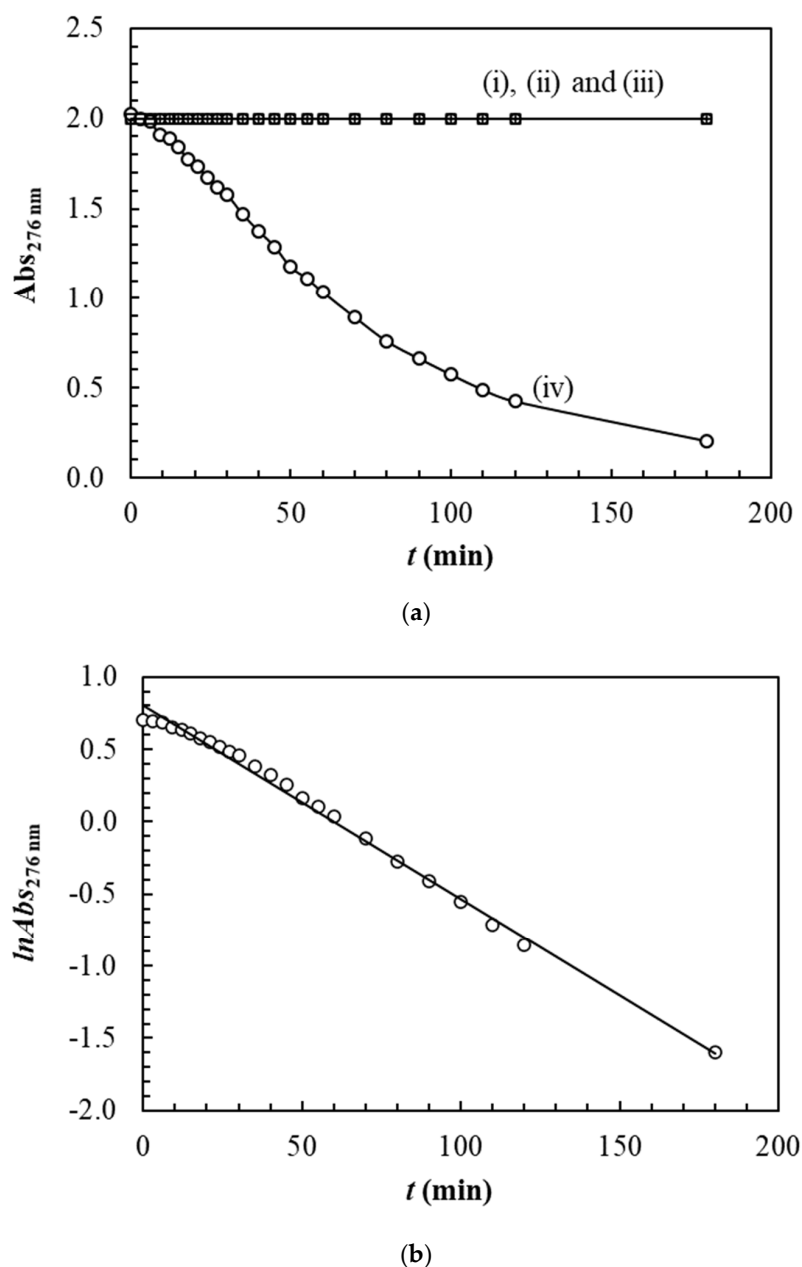


Figure 6. (a) Plots of A_{276nm} vs. t for CPF degradation in aqueous solution for various control experiments: (i) 50 μ M CPF + CS-GLA immobilized on a glass plate + solar light; (ii) 50 μ M CPF + Fe^{III} -CS-GLA immobilized on a glass plate + solar light; (iii) 50 μ M CPF + Fe^{III} -CS-GLA immobilized on a glass plate + H_2O_2 + dark; (iv) 50 μ M CPF + Fe^{III} -CS-GLA immobilized on a glass plate + H_2O_2 + solar light. (b) Plot of $\ln A_{276nm}$ vs. t for oxidative degradation of CPF in aqueous solution at optimum condition (control (iv)). Experimental conditions: $[CPF]_0$: 50 μ M; $[Fe^{III}]_0$ in Fe^{III} -CS-GLA: 1.25 mM; $[GLA]_0$ in Fe^{III} -CS-GLA: 90 mM; $[H_2O_2]_0$: 6 mM; volume of CPF solution: 250 mL; pH: 3; light intensity: 70,000–90,000 Lux; solar light irradiation time: 180 min.

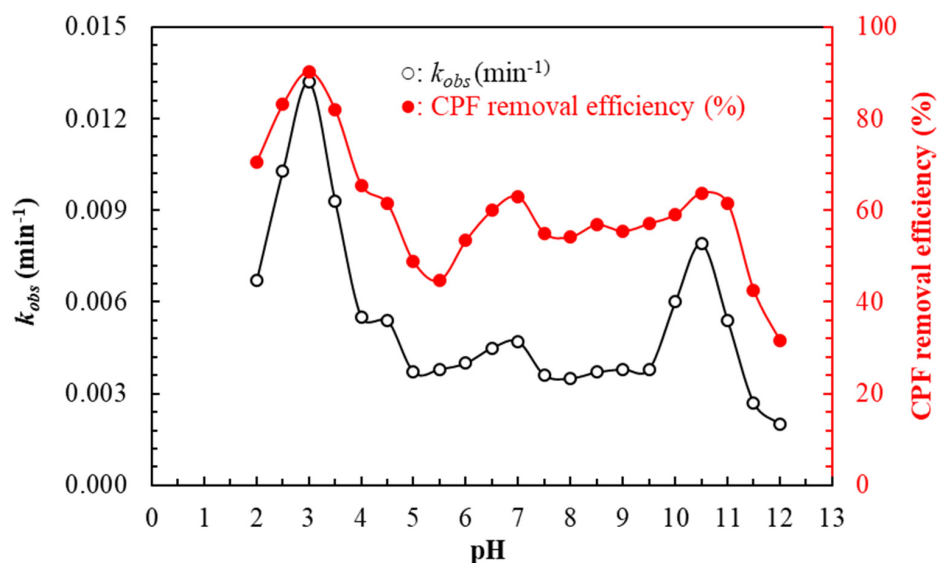


Figure 7. The effects of pH on k_{obs} (min^{-1}) and CPF removal efficiency (%) observed in solar light-assisted oxidative degradation of CPF catalyzed by Fe^{III} -CS-GLA in aqueous solution. Experimental conditions: $[\text{CPF}]_0$: 50 μM ; $[\text{Fe}^{\text{III}}]_0$ in Fe^{III} -CS-GLA: 1.25 mM; $[\text{GLA}]_0$ in Fe^{III} -CS-GLA: 90 mM; $[\text{H}_2\text{O}_2]_0$: 6 mM; volume of CPF solution: 250 mL; pH: 2–12; light intensity: 70,000–90,000 Lux; solar light irradiation time: 180 min.

2.2.3. Effect of GLA Dosage in Fe^{III} -CS-GLA

CS is frequently crosslinked with glutaraldehyde to enrich its mechanical strength, heat resistance, and chemical stability [55]. Usually, natural CS dissolves under acidic pH conditions, and cross-linking could help its application at low pH. The effects of cross-linking density in Fe^{III} -CS-GLA immobilized on a glass plate were investigated by measuring the CPF degradation rate constants (k_{obs}) and CPF removal efficiency in aqueous solution (pH 3) with a fixed initial concentration of CPF (50 μM) and H_2O_2 (6 mM) for 180 min. The effects of cross-linking density in Fe^{III} -CS-GLA on k_{obs} and CPF removal efficiency are shown in Figure 8. It is evident that the values of k_{obs} and CPF removal efficiency increase with increasing concentration of GLA up to 90 mM in Fe^{III} -CS-GLA, which may be due to the increase of Fe^{III} content on the surface of the Fe^{III} -CS-GLA material, leading to more production of the $\bullet\text{OH}$ reactive species [46]. However, the kinetic rate constant (k_{obs}) and CPF removal efficiency decrease significantly as the GLA dosage in Fe^{III} -CS-GLA is continuously increased to 120 mM. This may be due to the increase in Schiff base formation as a result of the reaction between the aldehyde group of glutaraldehyde and the $-\text{NH}_2$ groups of CS, leading to diminished complexation of Fe^{III} through the $-\text{NH}_2$ binding sites of CS. For CS microspheres loaded with gadolinium diethylenetriaminopentaacetic acid, some of us previously found that the size distribution and gadolinium content were influenced by the cross-linking density of the CS [56]. Therefore, all further solar light-assisted oxidative CPF degradation experiments at pH 3 were carried out with Fe^{III} -CS-GLA (immobilized on a glass plate) synthesized using 90 mM of GLA.

2.2.4. Effect of Iron(III) Content in Fe^{III} -CS-GLA

Figure 9 shows the change in CPF degradation rate constant (k_{obs}) and CPF removal efficiency at various Fe^{III} contents in Fe^{III} -CS-GLA immobilized on a glass plate with a fixed initial concentration of CPF (50 μM) and H_2O_2 (6 mM) after 180 min. It is noticed that the values of k_{obs} and CPF removal efficiency increase with increasing Fe^{III} content, from 0.0134 min^{-1} and 90.3% for 1.25 mM to 0.0230 min^{-1} and 98.0% for 7.5 mM Fe^{III} content in the Fe^{III} -CS-GLA catalyst. These may be due to the increase of $\bullet\text{OH}$ radical production with increasing Fe^{III} content, where $\bullet\text{OH}$ radicals control the rate of the CPF degradation reaction. Hence, a high concentration of Fe^{III} in Fe^{III} -CS-GLA is beneficial for high degradation rates

and high CPF removal efficiency. Similar results were also observed in the photo-assisted mineralization of ciprofloxacin by using a modified laponite clay-based Fe nanocomposite (Fe-Lap-RD) as a heterogeneous catalyst in the presence of H_2O_2 and UV light [36], in the oxidative degradation of trichloroethylene via a modified Fenton reaction using Fe^{II} chelated with cross-linked CS [46], and in the degradation of alachlor with Fe^{II} -citrate in a photo-Fenton reaction [57]. For all further CPF degradation experiments of the present study, the iron concentration in the Fe^{III} -CS-GLA catalyst immobilized on a glass plate was kept at 1.25 mM.

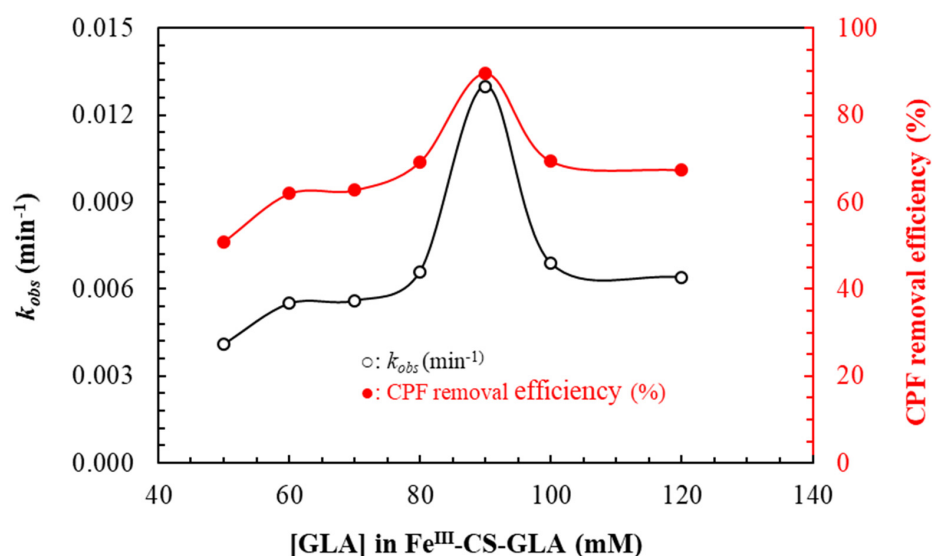


Figure 8. The effects of $[\text{GLA}]_0$ in Fe^{III} -CS-GLA on k_{obs} (min^{-1}) and CPF removal efficiency (%) observed in solar light-assisted oxidative degradation of CPF catalyzed by Fe^{III} -CS-GLA in aqueous solution. Experimental conditions: $[\text{CPF}]_0$: 50 μM ; $[\text{Fe}^{\text{III}}]_0$ in Fe^{III} -CS-GLA: 1.25 mM; $[\text{GLA}]_0$ in Fe^{III} -CS-GLA: 50–120 mM; $[\text{H}_2\text{O}_2]_0$: 6 mM; volume of CPF solution: 250 mL; pH: 3; light intensity: 70,000–90,000 Lux; solar light irradiation time: 180 min.

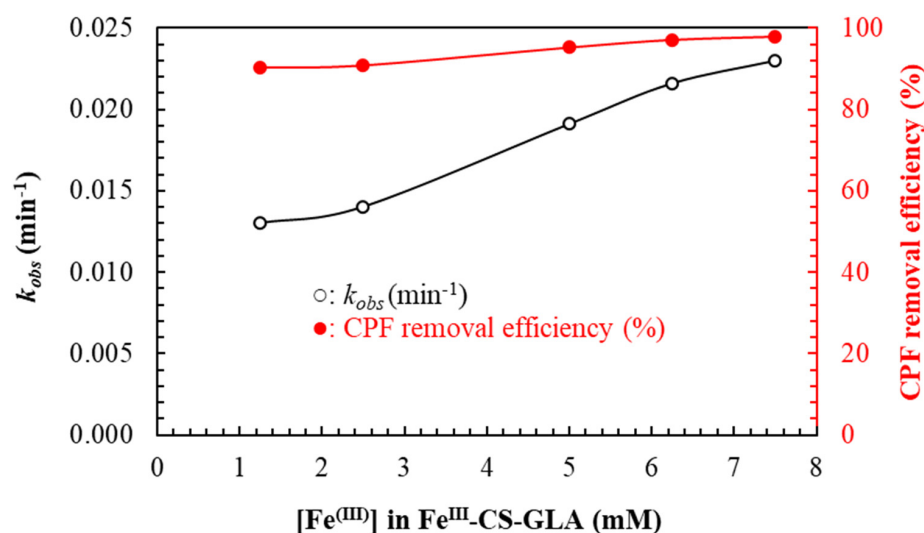


Figure 9. The effects of $[\text{Fe}^{\text{III}}]$ content in Fe^{III} -CS-GLA on k_{obs} (min^{-1}) and CPF removal efficiency (%) observed in solar light-assisted oxidative degradation of CPF catalyzed by Fe^{III} -CS-GLA in aqueous solution. Experimental conditions: $[\text{CPF}]_0$: 50 μM ; $[\text{Fe}^{\text{III}}]_0$ in Fe^{III} -CS-GLA: 1.25–7.50 mM; $[\text{GLA}]_0$ in Fe^{III} -CS-GLA: 90 mM; $[\text{H}_2\text{O}_2]_0$: 6 mM; volume of CPF solution: 250 mL; pH: 3; light intensity: 70,000–90,000 Lux; solar light irradiation time: 180 min.

2.2.5. Effect of H₂O₂ Concentration

It has been reported that the H₂O₂ concentration is directly related to the number of hydroxyl radicals generated in the photo-Fenton reaction for the degradation of organic compounds [36]. In the present study, it is found that the H₂O₂ concentration is one of the dominant control parameters for the solar light-assisted oxidative degradation of CPF by Fe^{III}-CS-GLA in aqueous solution (pH 3). The effect on k_{obs} and on the CPF removal efficiency was studied by varying the H₂O₂ concentrations in the range 1–12 mM while keeping fixed the initial concentration of CPF (50 μM) and the Fe^{III} content in the Fe^{III}-CS-GLA catalyst (1.25 mM); the results are shown in Figure 10. Both the values of k_{obs} and the CPF removal efficiency increase with increasing concentration of H₂O₂ from 1 mM H₂O₂ ($k_{obs} = 0.0090 \text{ min}^{-1}$, 79.7% CPF removal efficiency) to 6 mM H₂O₂ ($k_{obs} = 0.0134 \text{ min}^{-1}$, 90.3%). This is likely due to the formation of more hydroxyl radicals at higher H₂O₂ concentrations, which increases the degradation rate of CPF [36]. However, the values of k_{obs} and CPF removal efficiency then level off at even higher H₂O₂ concentrations, reaching $k_{obs} = 0.0150 \text{ min}^{-1}$ and 91.8% for 12 mM H₂O₂. This phenomenon might be explained by the scavenging effect of excess H₂O₂, which attenuates the number of •OH radicals in the solution. These results are in accordance with previous findings for the degradation of ciprofloxacin [36] and azo dyes such as Orange II [58], reactive red HE-3B [59] and acid black 1 [60] catalyzed by Fe-Lap-RD in the presence of H₂O₂ and UV light. Therefore, the H₂O₂ concentration was kept at 6 mM for further CPF degradation experiments using the Fe^{III}-CS-GLA immobilized on a glass plate (at pH 3).

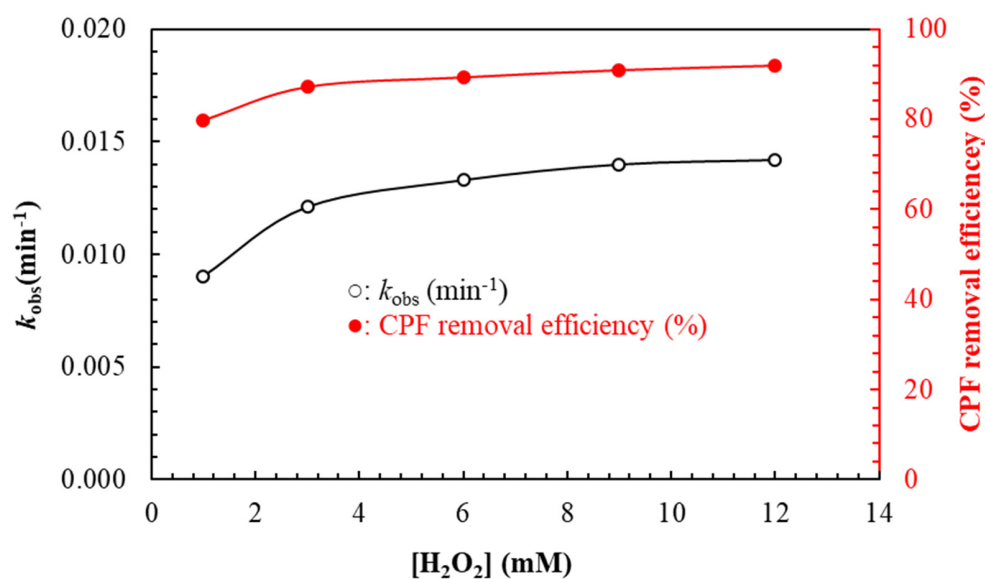


Figure 10. The effects of H₂O₂ concentration on k_{obs} (min⁻¹) and CPF removal efficiency (%) observed in the solar light-assisted oxidative degradation of CPF catalyzed by Fe^{III}-CS-GLA in aqueous solution. Experimental conditions: [CPF]₀: 50 μM, [Fe^{III}]₀ in Fe^{III}-CS-GLA: 1.25 mM; [GLA]₀ in Fe^{III}-CS-GLA: 90 mM; [H₂O₂]₀: 1–12 mM; volume of CPF solution: 250 mL; pH: 3; light intensity: 70,000–90,000 Lux; solar light irradiation time: 180 min.

2.2.6. Effect of CPF Concentration

To examine the effect of substrate concentrations on the degradation rate, the CPF concentration was varied in the range 20–50 μM under standard conditions established in the experiments described above (1.25 mM Fe^{III} content in Fe^{III}-CS-GLA immobilized on a glass plate, 6 mM H₂O₂, pH 3, and 180 min reaction time). The CPF degradation rate constant (k_{obs}) and the CPF removal efficiency decrease with increasing initial CPF concentration (Figure 11), from $k_{obs} = 0.0183 \text{ min}^{-1}$ and 95.0% for a 20 μM CPF solution to $k_{obs} = 0.0134 \text{ min}^{-1}$ and 90.3% for a 50 μM CPF solution. However, the overall CPF degradation rate increases with increasing initial CPF concentration. A likely reason for

these observations is that the concentration of hydroxyl radicals remains constant for all CPF molecules when the CPF concentration is increased, leading to a net decrease of k_{obs} and the removal efficiency [61]. It was also reported that the CPF degradation rate constant (k_{obs}) gradually decreases with increasing initial CPF concentration because of the increase in Cl^- concentration, since Cl^- scavenges the hydroxyl radicals and results in prolonged reaction times [43]. Formation of inorganic radical anions ($\text{Cl}^- + \bullet\text{OH} \rightarrow \text{ClOH}\bullet^-$) is possible under these conditions. Although the reactivity of the latter radical may be relevant, it is not as reactive as $\bullet\text{OH}$, and thus the observed retardation effect is thought to be caused by strong adsorption of the anions on the Fe^{III} -CS-GLA surface [43].

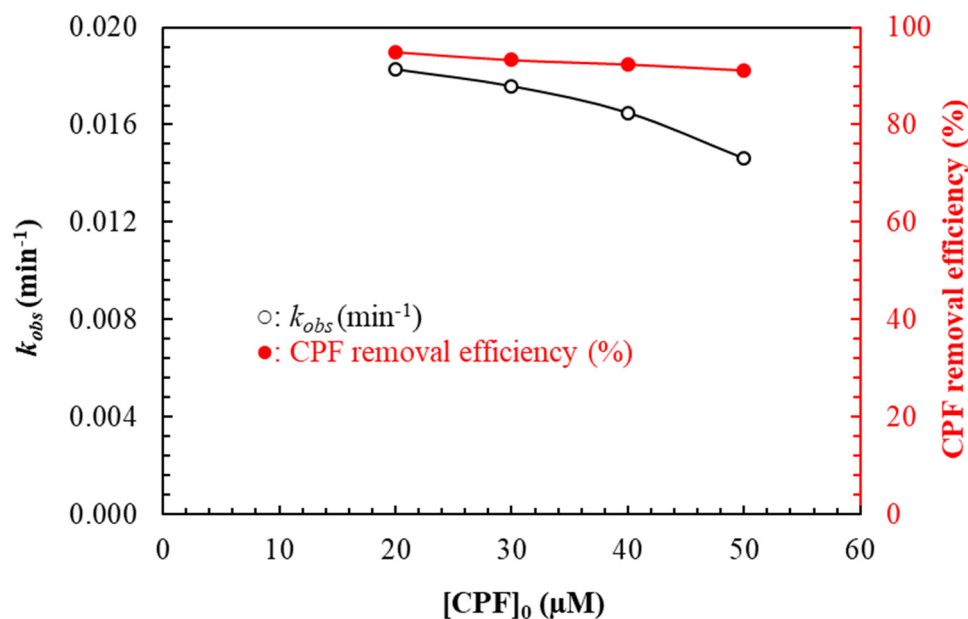


Figure 11. The effect of CPF concentration on k_{obs} (min^{-1}) and CPF removal efficiency (%) observed in the solar light-assisted oxidative degradation of CPF catalyzed by Fe^{III} -CS-GLA in aqueous solution. Experimental conditions: $[\text{CPF}]_0$: 20–50 μM ; $[\text{Fe}^{\text{III}}]_0$ in Fe^{III} -CS-GLA: 1.25 mM; $[\text{GLA}]_0$ in Fe^{III} -CS-GLA: 90 mM; $[\text{H}_2\text{O}_2]_0$: 6 mM; volume of CPF solution: 250 mL; pH: 3; light intensity: 70,000–90,000 Lux; solar light irradiation time: 180 min.

It has previously been proposed that the kinetics for the heterogeneous catalytic antibiotic degradation processes follow a Langmuir-Hinshelwood (LH) model [43,62], which implies that both molecules adsorb on the catalyst surface where they undergo a bimolecular reaction, in this case between the hydroxyl radical ($\bullet\text{OH}$) and CPF. The Langmuir-Hinshelwood model of heterogeneous catalytic CPF degradation systems is given by:

$$\text{Rate} = -\frac{d[\text{CPF}]}{dt} = \frac{kK_{\text{CPF}}[\text{CPF}]}{1 + K_{\text{CPF}}[\text{CPF}]_0} = k_{obs}[\text{CPF}] \quad (1)$$

$$\frac{1}{k_{obs}} = \frac{1}{kK_{\text{CPF}}} + \frac{[\text{CPF}]_0}{k} \quad (2)$$

In Equations (1) and (2), $[\text{CPF}]_0$ (μM) is the initial concentration of ciprofloxacin, K_{CPF} ($\text{L} \cdot \mu\text{mol}^{-1}$) is the Langmuir-Hinshelwood adsorption equilibrium constant, k ($\mu\text{mol} \cdot \text{L}^{-1} \cdot \text{min}^{-1}$) is the rate constant of the surface reaction, and k_{obs} (min^{-1}) is the pseudo-first-order rate constant. According to Equation (2), a plot of $\frac{1}{k_{obs}}$ vs. $[\text{CPF}]_0$ is a straight line with slope $\left(\frac{1}{k}\right)$ and intercept $\left(\frac{1}{kK_{\text{CPF}}}\right)$. Applying this model to the present system gives $k = 2.2060 \mu\text{mol} \cdot \text{L}^{-1} \cdot \text{min}^{-1}$ and $K_{\text{CPF}} = 0.0102 \text{L} \cdot \mu\text{mol}^{-1}$ ($R^2 = 0.9238$; see Figure 12). This result suggests that the solar-light assisted degradation of CPF catalyzed by Fe^{III} -CS-GLA immobilized on a glass plate is

well described by the Langmuir-Hinshelwood kinetics model, and the substrate degradation mechanism occurs via adsorption steps on the catalyst [43,62].

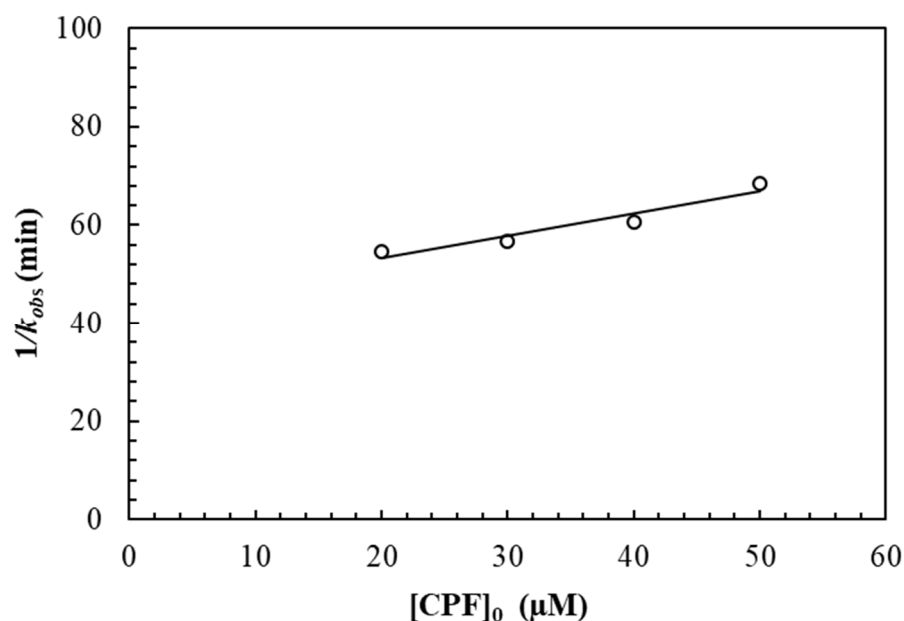


Figure 12. Plot of $1/k_{obs}$ vs. initial concentration of CPF.

2.2.7. Effect of a Hydroxyl Radical Scavenger

To further investigate the degradation mechanism, the oxidative decomposition of CPF catalyzed by Fe^{III}-CS-GLA was evaluated in aqueous solution under the optimized reaction conditions in presence of the specific hydroxyl radical scavenger mannitol [63]. The changes in k_{obs} values and CPF removal efficiency as a function of mannitol concentration are depicted in Figure 13. It is noticed that the values of k_{obs} and the removal efficiency of CPF significantly decrease upon addition of mannitol, corroborating that hydroxyl radicals (\bullet OH) are involved in the CPF degradation process. However, the values of k_{obs} and the removal efficiency of CPF remain at 0.0019 min^{-1} and 29%, respectively, at the highest concentration of mannitol (Figure 13), suggesting that the CPF initially adsorbs onto the catalyst surface followed by oxidative degradation via hydroxyl radicals (\bullet OH), as was also observed in photocatalytic oxidation of CPF under simulated sunlight [43].

2.2.8. Identification of the Oxidative Degradation Products of CPF

HPLC-UV-ESI-MS investigations were performed to identify residual amounts of CPF together with the degradation products obtained from the solar-light assisted oxidative degradation of CPF catalyzed by Fe^{III}-CS-GLA in the presence of H₂O₂ in aqueous solution, using the standard conditions established in this work; the resulting chromatograms are shown in Figure S3. Three major peaks with different retention times are detected in the ESI-MS(–) (Figure S3a) and UV-based (Figure S3b) chromatograms. The degradation products identified in the reaction solution are specified in Table 2. Compounds 1 (C₅H₈O₅) and 3 (C₅H₈O₄) are hydroxy glutaric acid and glutaric acid, respectively, as confirmed by the measurement of those compounds as reference substances (see supporting information); these two products likely originate from the oxidative degradation of the Schiff base crosslinking units formed in the reaction between glutaraldehyde and chitosan. The identity of degradation product 2 as succinic acid was also confirmed by measurement of a reference sample. Applying HPLC-UV-ESI(+)-MS analysis in the positive ion mode, CPF as a reference compound is detected with a retention time of 13.18 min (see supporting information). However, no such signal for intact CPF was found in the HPLC-UV-ESI-MS traces after oxidative treatment, neither in the positive nor in the negative ion mode, confirming complete degradation of the substrate.

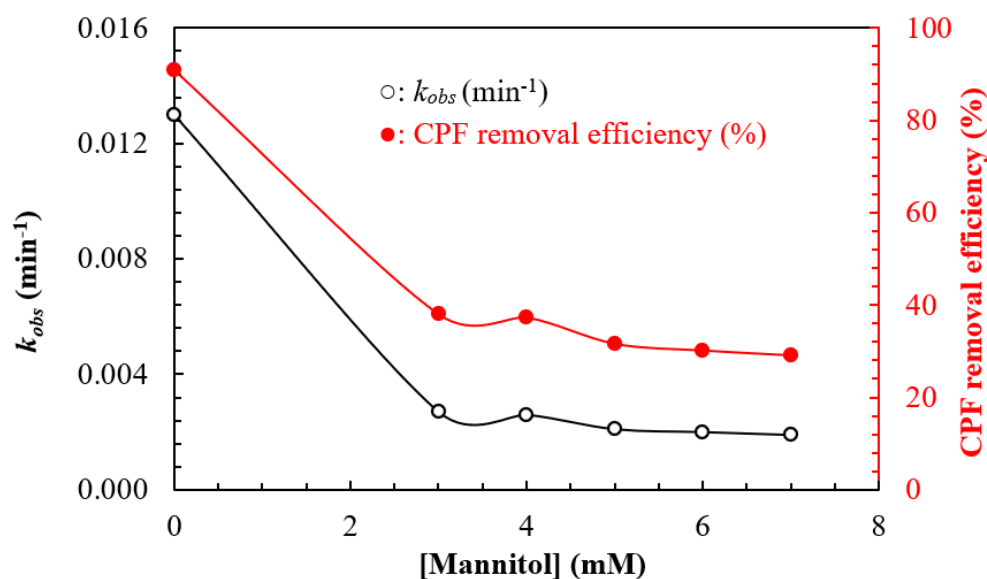


Figure 13. The effects of mannitol concentration on k_{obs} (min^{-1}) and CPF removal efficiency (%) observed in solar light-assisted oxidative degradation of CPF catalyzed by Fe^{III} -CS-GLA in aqueous solution. Experimental conditions: $[\text{CPF}]_0$: 50 μM , $[\text{Fe}^{\text{III}}]_0$ in Fe^{III} -CS-GLA: 1.25 mM, $[\text{GLA}]_0$ in Fe^{III} -CS-GLA: 90 mM, $[\text{H}_2\text{O}_2]_0$: 6 mM, $[\text{Mannitol}]$: 0–7 mM, volume of CPF solution: 250 mL, pH: 3, light intensity: 70,000–90,000 Lux, solar light irradiation time: 180 min.

Table 2. Compounds detected by HPLC-ESI(-)-MS after solar light-assisted oxidative degradation of CPF in aqueous solution catalyzed by Fe^{III} -CS-GLA in presence of H_2O_2 .

No.	$t_{\text{(R)}}$ min	m/z	Elemental Composition	Proposed Compound
1	2.5	147.0300 $[\text{M}-\text{H}]^-$	$\text{C}_5\text{H}_7\text{O}_5$	$\text{C}_5\text{H}_8\text{O}_5$
		129.0194 $[\text{M}-\text{H}-\text{H}_2\text{O}]^-$	$\text{C}_5\text{H}_5\text{O}_4$	Hydroxy-pentanedioic acid
2	3.0	117.0195 $[\text{M}-\text{H}]^-$	$\text{C}_4\text{H}_5\text{O}_4$	$\text{C}_4\text{H}_6\text{O}_4$
				Butanedioic acid
3	4.0	131.0350 $[\text{M}-\text{H}]^-$	$\text{C}_5\text{H}_7\text{O}_4$	$\text{C}_5\text{H}_8\text{O}_4$
				Pentanedioic acid

2.2.9. Antibacterial Activity of CPF before and after Catalytic Degradation

The antibacterial activity of CPF in the concentration range 50–200 μM was investigated against both Gram-negative (i.e., *Escherichia coli* DH5 α and *Salmonella typhi* AF450) and Gram-positive (i.e., *Bacillus subtilis* RBW) bacteria before and after treatment with Fe^{III} -CS-GLA/ H_2O_2 under the standard conditions developed above. The typical zone of inhibition observed for each bacterium for various CPF solutions before and after catalytic degradation is shown in Figure 14, and the antibacterial activities are listed in Table 3. The pristine CPF solutions, before catalytic CPF degradation, significantly inhibit the growth of both Gram-negative (i.e., *Escherichia coli* DH5 α and *Salmonella typhi* AF450) and Gram-positive (i.e., *Bacillus subtilis* RBW) bacteria. However, no zone of inhibition was observed for any of the bacteria after treatment with Fe^{III} -CS-GLA/ H_2O_2 , which indicates that the CPF was completely degraded during the process. This is in line with the absence of any CPF in the HPLC-UV-ESI-MS analyses of samples that had undergone the oxidative treatment, and the findings suggest complete mineralization of CPF with Fe^{III} -CS-GLA/ H_2O_2 in the presence of solar light in aqueous solution [36].

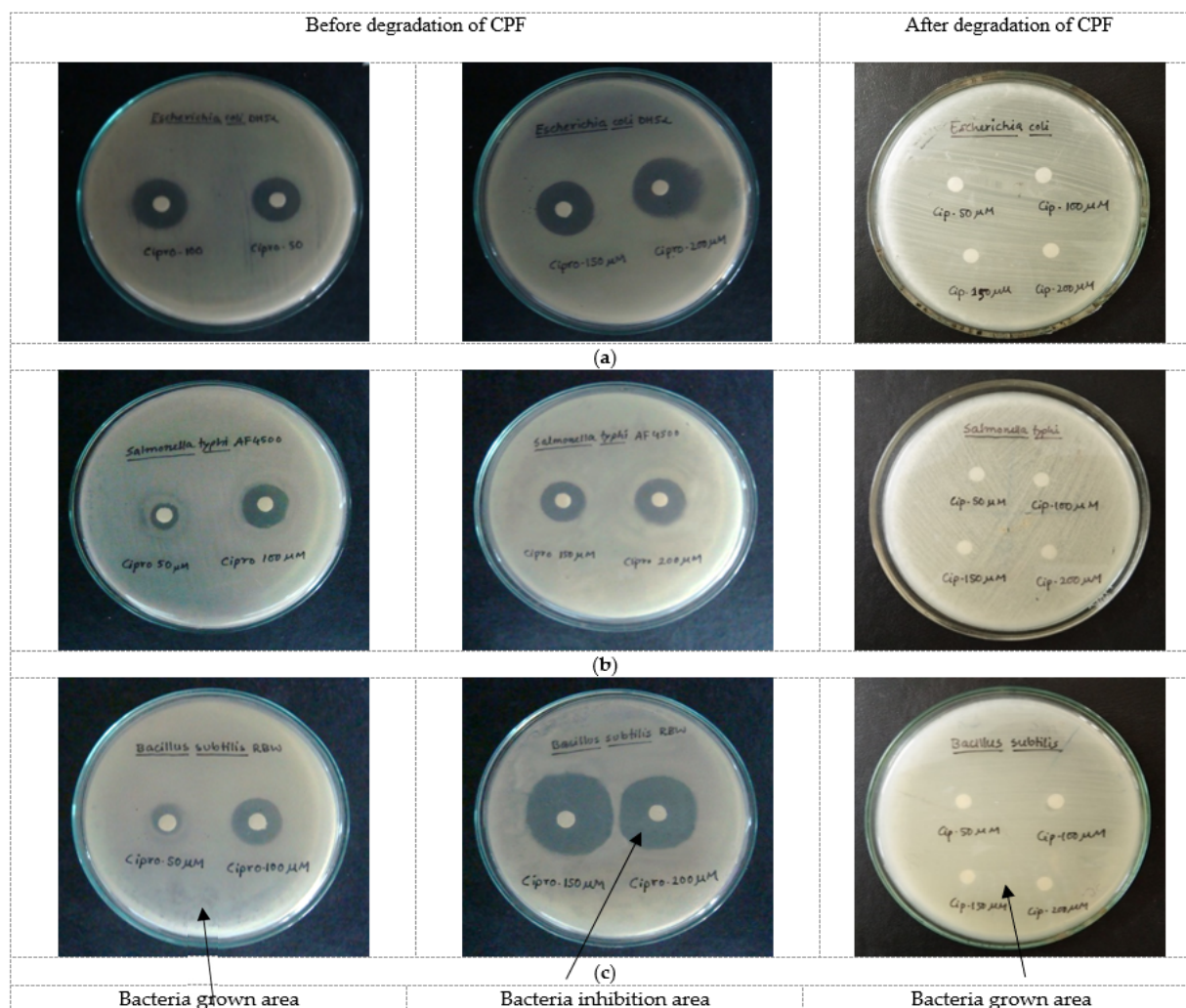


Figure 14. Antimicrobial activity of CPF (from left to right: 50, 100, 150, and 200 μM) against (a) *Escherichia coli* DH5 α , (b) *Salmonella typhi* AF4500 and (c) *Bacillus subtilis* RBW bacteria before and after solar light-assisted oxidative treatment with Fe^{III} -CS-GLA/ H_2O_2 in aqueous solution.

Table 3. Antibacterial activities of CPF before and after catalytic degradation with Fe^{III} -CS-GLA/ H_2O_2 against *Escherichia coli* DH5 α , *Salmonella typhi* AF4500 and *Bacillus subtilis* RBW bacteria.

Concentration of CPF (μM)	Zone of Inhibition (mm) for Test Bacteria		
	<i>Escherichia coli</i> DH5 α	<i>Salmonella typhi</i> AF4500	<i>Bacillus subtilis</i> RBW
Before catalytic degradation of CPF			
50	16.20 \pm 0.40	10.00 \pm 0.72	9.30 \pm 1.10
100	18.10 \pm 0.72	13.40 \pm 0.68	16.60 \pm 0.20
150	19.60 \pm 0.50	15.10 \pm 0.56	22.20 \pm 0.10
200	20.40 \pm 0.71	24.30 \pm 0.40	25.10 \pm 0.98
After catalytic degradation of CPF			
50	Not detected	Not detected	Not detected
100	Not detected	Not detected	Not detected
150	Not detected	Not detected	Not detected
200	Not detected	Not detected	Not detected

2.2.10. Reuse of the Fe^{III} -CS-GLA Catalyst for Degradation of CPF in Aqueous Solution

In order to examine the reusability of the catalyst, the CPF degradation using Fe^{III} -CS-GLA immobilized on a glass plate was studied for four consecutive cycles (Figure 15). The CPF removal efficiency decreases slightly after repeated use of the Fe^{III} -CS-GLA catalyst:

after three and four runs, the CPF removal decreased from 90% to 80%, 72% and finally 63%, respectively. This might be due to the gradual leaching of iron ions as well as the loss of cross-linking density during the degradation process. The leaching of iron from Fe^{III}-CS-GLA is corroborated by the changes in iron mass percentage found in the EDX analysis of the immobilized catalyst before and after CPF degradation (Figure S2a,b). Similarly, observation of the degradation products glutaric acid and hydroxy glutaric acid (Table 2) evidence the loss of cross-linking density in the Fe^{III}-CS-GLA during the CPF degradation process. Overall, however, the synthesized Fe^{III}-CS-GLA system was found to exhibit reasonable catalytic stability with only moderate loss of catalytic activity during repeated use for oxidative CPF degradation, and hence it shows good promise as a relatively stable and efficient photo-Fenton catalyst.

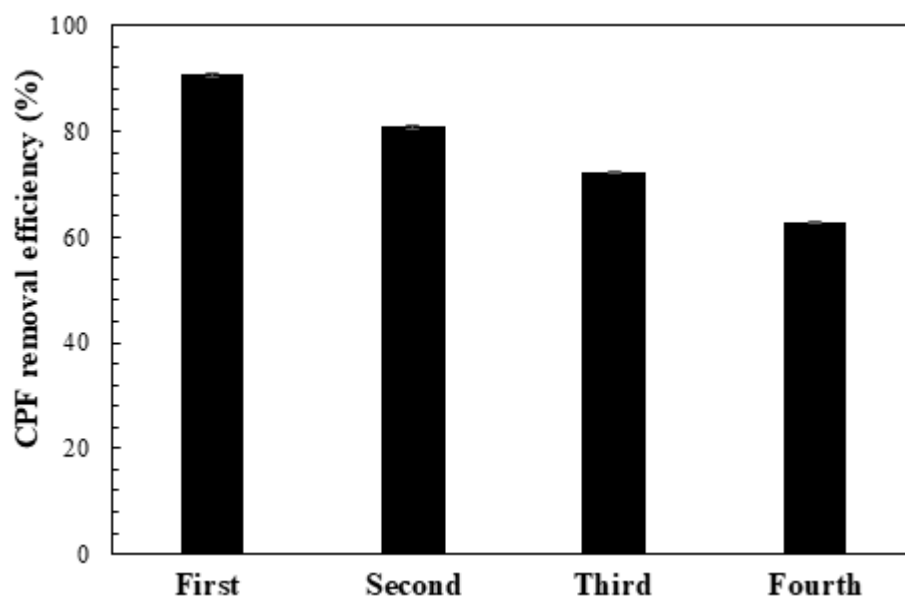


Figure 15. Efficiency of the Fe^{III}-CS-GLA catalyst during repeated use for solar light-assisted oxidative degradation of CPF in aqueous solution. Experimental conditions: [CPF]₀: 50 μM; [Fe^{III}]₀ in Fe^{III}-CS-GLA: 1.25 mM; [GLA]₀ in Fe^{III}-CS-GLA: 90 mM; [H₂O₂]₀: 6 mM; volume of CPF solution: 250 mL; pH: 3; light intensity: 70,000–90,000 Lux; solar light irradiation time: 180 min.

3. Materials and Methods

3.1. Materials and Reagents

Ciprofloxacin hydrochloride was purchased from Sigma-Aldrich, Germany and used as received. Chitosan (Sigma-Aldrich, Stuttgart, Germany), acetic acid (MERCK, Darmstadt, Germany), ferrous chloride tetrahydrate (FeCl₂·4H₂O; Sigma-Aldrich), glutaraldehyde (GLA; MERCK), analytical-grade H₂O₂ (35% in solution, Merck), mannitol (Sigma-Aldrich), hydrochloric acid (MERCK, Germany), sodium hydroxide (MERCK), deionized water, Müller-Hinton agar powder (Becon, Courbevoie, France), peptone (Becon), yeast extract (UNI-CHEM, Wuxi, China) etc. were used for this study in extremely pure form and used as received without further purification.

3.2. Preparation of Iron(III) Chelated Cross-Linked Chitosan, Fe^{III}-CS-GLA, Immobilized on a Glass Plate

The Fe^{III}-CS-GLA immobilized on a glass plate was prepared according to the method reported by Lee and Lee [46] with minor modifications. To prepare the chitosan solution, an exact amount (0.2 g) of chitosan was dissolved in 100 mL of 5% (v/v) acetic acid in a volumetric flask, and the solution was stirred with a magnetic stirrer at 250 rpm overnight. The required amount (0.7455 g) of FeCl₂·4H₂O was dissolved in 25 mL of 5% (v/v) acetic acid to prepare a 150 mM iron containing stock solution. Then, the required volume of this iron stock solution was mixed with the chitosan solution under magnetic stirring

at 250 rpm for 1 h at room temperature (30 °C) to prepare solution A. Glutaraldehyde (GLA) was added to solution A with stirring to prepare the final solution B. To prepare the catalyst samples, an equal number of droplets of solution B was then deposited on the previously weighted glass slide (76 mm × 30 mm × 3 mm; previously cleaned with dilute HCl solution and ethanol), and the glass slides were heated at 100 °C for 2 h in an electronic oven to anneal the chitosan film. After that, the glass side with the catalyst films were cooled to room temperature and washed with deionized water. Finally the glass plates with immobilized Fe^{III}-CS-GLA were dried again and stored in a desiccator to avoid the absorption of moisture. Different catalyst samples for the experiments described in this publication were prepared by varying the concentration of GLA (50–120 mM) and Fe^{III} content (1.25–7.50 mM) in the Fe^{III}-CS-GLA, respectively.

3.3. Characterization of Fe^{III}-CS-GLA

The Fe^{III}-CS-GLA catalyst was characterized by Fourier transform infra-red (FTIR) and [57] Fe Mössbauer spectroscopies, field emission scanning electron microscopy (FE-SEM) analysis coupled with energy dispersive X-ray spectroscopy (EDX), as well as X-ray diffraction (XRD). The FTIR spectra of chitosan and Fe^{III}-CS-GLA were recorded in KBr in the range of 400–4000 cm⁻¹ using a SHIMADZU Prestige-21 spectrometer (Japan). Mössbauer spectra of Fe^{III}-CS-GLA were recorded with a [57] Co source in a Rh matrix using an alternating constant acceleration Wissel Mössbauer spectrometer operated in the transmission mode and equipped with a Janis closed-cycle helium cryostat. Isomer shifts are given relative to iron metal at ambient temperature. Simulation of the experimental data was performed with the Mfit program using Lorentzian line doublets [64]. FE-SEM analysis of the surface morphology of the materials was performed using a JSM-7610F Schottky field emission scanning electron microscope (JEOL Ltd., Japan) equipped with EDX at an accelerating voltage of 15 kV. The crystallinity of the samples was investigated by using an X-ray diffractometer (GNR-EXPLORER, GNR Analytical Instruments Group, Macerata, Italy) with Cu-K α radiation ($\lambda = 1.54056 \text{ \AA}$) at 30 kV and 20 mA.

3.4. Fe^{III}-CS-GLA Catalyzed Batch Oxidative Degradation of CPF in Aqueous Solution

The degradation of CPF was carried out in a batch reaction system under open air on the roof of the Department of Chemistry at Jahangirnagar University between 11 am to 2 pm on sunny days. In order to explore the suitable condition for CPF elimination from aqueous solution, the following control experiments were executed in aqueous solution at pH 3:

- (i) 50 μM CPF + CS-GLA immobilized on a glass plate + solar light;
- (ii) 50 μM CPF + Fe^(III)-CS-GLA immobilized on a glass plate + solar light;
- (iii) 50 μM CPF + Fe^(III)-CS-GLA immobilized on a glass plate + H₂O₂ + dark;
- (iv) 50 μM CPF + Fe^(III)-CS-GLA immobilized on a glass plate + H₂O₂ + solar light.

In batch degradation experiments, 250 mL of 50 μM CPF solution was taken in a 1000 mL beaker. The pH of antibiotic solution was adjusted with 1 M HCl or NaOH solution and measured by using a pH meter (Adwa AD8000). The Fe^(III)-CS-GLA immobilized on the glass plate was placed in the beaker containing 6 mM H₂O₂ with 50 μM CPF solution and was irradiated directly with sunlight of intensity between 70,000 to 90,000 Lux (URCERI MT-912 digital Lux meter) for oxidative degradation. After a definite time interval, a certain portion of the irradiated solution (3 mL) was collected and returned to the beaker after it was scanned in the range from 500 nm to 190 nm using a Shimadzu UV-1800 spectrophotometer (Shimadzu, Japan). The volume of the reaction mixture was kept constant during the experiment. The absorbance of CPF at $\lambda_{\text{max}} = 276 \text{ nm}$ was monitored and used in the kinetics analysis [32]. The apparent molar absorptivity of CPF was estimated to be 0.0399 L· μM^{-1} ·cm⁻¹ at 276 nm.

The CPF removal efficiency (%) was calculated by the following equation (3): [42]

$$\text{CPF removal efficiency (\%)} = \frac{A_0 - A_t}{A_0} \times 100 \quad (3)$$

where A_0 and A_t are the absorbance of the CPF solution at 276 nm at initial time and at any time t , respectively.

The observed pseudo-first-order rate constant (k_{obs}) was determined from the slope of the straight line Equation (4): [65]

$$\ln A_t = \ln A_0 - k_{obs} t \quad (4)$$

where A_0 and A_t are same as in Equation (3).

The CPF degradation kinetics were also determined after varying the solution pH (2–12), concentration of GLA in Fe^{III}-CS-GLA (50–120 mM), Fe^{III} content in Fe^{III}-CS-GLA (1.25–7.50 mM), concentration of H₂O₂ (1–12 mM), concentration of CPF (20–50 μM), and concentration of the added hydroxyl radical ([•]OH) scavenger mannitol (0–7 mM), respectively. After catalytic degradation of CPF, the Fe^{III}-CS-GLA catalyst was withdrawn from the reaction mixture and washed several times with deionized water to remove remaining substrate and its degradation products. Then, the Fe^{III}-CS-GLA catalyst was reused for the degradation of CPF in aqueous solution, and the amount of CPF degradation was determined in the same way as described above. All data presented in this paper are the average at least twofold measurements.

3.5. Investigation of the Products of Oxidative CPF Degradation by HPLC-UV-ESI-MS

HPLC-MS measurements were performed on a Thermo Fisher Scientific (Waltham, MA, USA) HPLC-MS system consisting of a Accela HPLC with a Finnigan Surveyor PDA Detector and coupled to a LTQ Orbitrap XL high resolution mass spectrometer (R~60,000) equipped with an electrospray ionization (ESI) source. Chromatographic separation was carried out using a Synergi Hydro-RP column (150 mm length, 2 mm inner diameter, 4 μm particle size, Phenomenex). An aliquot of the aqueous reaction solution (10 μL) and reference substance solutions were injected by the autoinjector. Water with 0.05 % formic acid (A) and methanol with 0.05 % formic acid (B) were used as eluents with a flow rate of 0.2 mL·min⁻¹ applying the following gradient elution: 0–2 min 90/10 A/B, 2–15 min to 50/50 A/B, 15–20 min to 10/90 A/B, 20–25 min 10/90 A/B. The oven temperature was set to 45 °C. UV spectra were acquired in the range of 200–390 nm. Mass spectrometric analyses were performed by applying electrospray ionization with a spray voltage of 5.0 kV (negative ion mode) resp. 4.0 kV (positive ion mode), with a sheath gas flow of 50 (arb units) and a capillary temperature of 275 °C in the m/z range from 100 to 1000.

3.6. Assay for Antibacterial Activity Measurement

All the test samples were investigated for their antimicrobial activity against both Gram-negative (i.e., *Escherichia coli* DH5α and *Salmonella typhi* AF450) and Gram-positive (i.e., *Bacillus subtilis* RBW) bacteria by a simple disc diffusion method [66]. Qualitative assays were performed to evaluate the antibacterial activity of ciprofloxacin (CPF) before and after catalytic degradation against the fully susceptible test organisms including pathogenic (*Salmonella typhi* AF4500) and non-pathogenic *Escherichia coli* DH5α (Gram-negative) and *Bacillus subtilis* RBW (Gram-positive). All plates were prepared in sterile petri dishes with Luria Bertani (LB) agar. LB agar was prepared with 1% peptone, 0.5% yeast extract, 1% sodium chloride and 1.5% agar maintaining pH 7. LB broth and LB agar were prepared for inoculation and the assay, respectively. All of them were sterilized properly using an autoclave at 121 °C for 15 min. After autoclaving, agar plates were prepared before the LB agar became solid. LB broth was cooled to room temperature for inoculation. An inoculation loop was then taken from the rack placed in a laminar air flow cabinet. The loop was heated in the blue flame of the Bunsen burner until it became hot, and it was then

allowed to cool for some time. The petri dish containing the microbial culture was then taken and an isolated colony was picked using the sterile inoculation loop and mixed in a tube containing 5 mL of LB broth. The tube was allowed to shake in a shaking water bath overnight at 120 rpm at 37 °C for optimum growth of the microorganisms. An amount of 100 µL of the bacterial suspension was then taken and spread properly in the agar plate. Sterile antimicrobial disks were taken and were made wet with the corresponding samples. Then, the disks were placed on the prepared culture plates and placed into an incubator upside down at 37 °C for overnight growth of the microorganisms. After incubation, the plate was taken from the incubator and the diameter of the inhibition zones (in mm scale) was measured and recorded.

4. Conclusions

An iron(III) chelated cross-linked chitosan catalyst immobilized on a glass plate, Fe^{III}-CS-GLA, was developed for the elimination of CPF from aqueous solutions using hydrogen peroxide as an oxidant in combination with solar light. The immobilized Fe^{III}-CS-GLA was characterized by FTIR, ⁵⁷Fe Mössbauer and EDX spectroscopies as well as X-ray diffraction, which evidenced the presence of iron(III) and Schiff base functional groups of the crosslinked CS-GLA matrix. The oxidative degradation of CPF in aqueous solution using this catalyst was investigated as a function of solar light irradiation time, solution pH, cross-linker dosages and Fe^{III} content in the Fe^{III}-CS-GLA hybrid material, as well as concentrations of H₂O₂ and CPF. The degradation of CPF was found to be more rapid and efficient in acidic medium than alkaline medium, with an optimum in aqueous solution at pH 3. The CPF removal rate constant (k_{obs}) increases at higher iron content in the Fe^{III}-CS-GLA catalyst but decreases at a higher initial concentration of CPF, while both k_{obs} and the CPF removal efficiency increase at the higher of H₂O₂ concentrations. The kinetics data were found to follow pseudo-first-order and Langmuir-Hinshelwood models, and the adsorption of CPF onto the surface of Fe^{III}-CS-GLA was confirmed in FE-SEM and EDX analyses. The specific hydroxyl radical scavenger mannitol significantly inhibits the degradation of CPF in aqueous solution, suggesting that hydroxyl radicals play a major role in the catalytic activity of the Fe^{III}-CS-GLA/H₂O₂/solar light system. The oxidative degradation of CPF was proven by HPLC-UV-ESI-MS analyses and by evaluating the antimicrobial activity against both Gram-negative and Gram-positive bacteria before and after treatment; no zone of inhibition was observed for any bacteria after treating the CPF solution with the newly developed Fe^{III}-CS-GLA/H₂O₂/solar light catalyst system. Furthermore, this readily available catalyst immobilized on a glass plate can be repeatedly used for at least four times without significant loss of catalytic efficiency. Thus, Fe^{III}-CS-GLA is a very promising hybrid material that may serve as a stable and efficient photo-Fenton catalyst for future applications towards the removal of CPF (and potentially other antibiotics) from aqueous solutions.

Supplementary Materials: The following are available online at <https://www.mdpi.com/article/10.3390/catal12050475/s1>, Figure S1. X-ray diffraction patterns of CS (a) and Fe^{III}-CS-GLA (b); Figure S2. EDX analysis of Fe^{III}-CS-GLA before (a) and after (b) its use in the catalytic degradation of CPF; Figure S3. HPLC-UV-ESI(-)-MS chromatograms of the products obtained from solar light-assisted oxidative degradation of CPF catalyzed by Fe^{III}-CS-GLA in aqueous solution. (a) ESI(-)-MS base peak chromatogram and (b) UV chromatogram (total scan). Experimental conditions: [CPF]0: 50 µM, [Fe^{III}]0 in Fe^{III}-CS-GLA: 1.25 mM, [GLA]0 in Fe^{III}-CS-GLA: 90 mM, [H₂O₂]0: 6 mM, volume of CPF solution: 250 mL, pH: 3, light intensity: 70000-90000 Lux, solar light irradiation time: 180 min.

Author Contributions: Conceptualization, T.K.S. and S.K.; methodology, S.S., T.K.S., S.K., Z.I., S.D. and H.F.; software, S.S., T.K.S., Z.I., S.D. and H.F.; validation, S.S., T.K.S., Z.I., S.D. and H.F.; formal analysis, S.S., T.K.S., Z.I., S.D. and H.F.; investigation, S.S., T.K.S., Z.I., S.D. and H.F.; resources, T.K.S. and F.M.; data curation, S.S., T.K.S., Z.I., S.D. and H.F.; writing—original draft preparation, S.S.; writing—review and editing, T.K.S., S.K., H.F. and F.M.; visualization, T.K.S. and F.M.; supervision, T.K.S., S.K. and F.M.; project administration, T.K.S. and F.M.; funding acquisition, T.K.S. and F.M. All authors have read and agreed to the published version of the manuscript.

Funding: This research was funded by the Ministry of Science and technology, Government of the People’s Republic of Bangladesh (grant number FY 2020-2021) and by the Alexander von Humboldt Foundation. The APC was funded by the Open Access Publication Funds of the University of Göttingen and the Alexander von Humboldt Foundation.

Acknowledgments: T.K.S. is grateful to the Ministry of Science and technology, Government of the People’s Republic of Bangladesh for a research grant (FY 2020-2021) and thanks the Alexander von Humboldt Foundation for supporting his research stays in Göttingen.

Conflicts of Interest: The authors declare no conflict of interest.

References

1. Aslam, B.; Wang, W.; Arshad, M.I.; Khurshid, M.; Muzammil, S.; Rasool, M.H.; Nisar, M.A.; Alvi, R.F.; Aslam, M.A.; Qamar, M.U.; et al. Antibiotic resistance: A rundown of a global crisis. *Infect. Drug Resist.* **2018**, *11*, 1645–1658. [[CrossRef](#)] [[PubMed](#)]
2. Rather, I.A.; Kim, B.C.; Bajpai, V.K.; Park, Y.-H. Self-medication and antibiotic resistance: Crisis, current challenges, and prevention. *Saudi J. Biol. Sci.* **2017**, *24*, 808–812. [[CrossRef](#)] [[PubMed](#)]
3. Harrower, J.; McNaughtan, M.; Hunter, C.; Hough, R.; Zhang, Z.; Helwig, K. Chemical fate and partitioning behavior of antibiotics in the aquatic environment—A review. *Environ. Toxicol. Chem.* **2021**, *40*, 3275–3298. [[CrossRef](#)] [[PubMed](#)]
4. Beek, T.A.D.; Weber, F.-A.; Bergmann, A.; Hickmann, S.; Ebert, I.; Hein, A.; Küster, A. Pharmaceuticals in the environment—Global occurrences and perspectives. *Environ. Toxicol. Chem.* **2016**, *35*, 823–835. [[CrossRef](#)]
5. Gothwal, R.; Shashidhar, T. Antibiotic pollution in the environment: A review. *Clean-Soil Air Water* **2015**, *43*, 479–489. [[CrossRef](#)]
6. Kuppasamy, S.; Kakarla, D.; Venkateswarlu, K.; Megharaj, M.; Yoon, Y.-E.; Lee, Y.B. Veterinary antibiotics (VAs) contamination as a global agro-ecological issue: A critical view. *Agric. Ecosyst. Environ.* **2018**, *257*, 47–59. [[CrossRef](#)]
7. Zhu, Y.-G.; Johnson, T.A.; Su, J.-Q.; Qiao, M.; Guo, G.-X.; Stedtfeld, R.-D.; Hashsham, S.A.; Tiedje, J.M. Diverse and abundant antibiotic resistance genes in Chinese swine farms. *Proc. Natl. Acad. Sci. USA* **2013**, *110*, 3435–3440. [[CrossRef](#)]
8. Munir, M.; Xagorarakis, I. Levels of antibiotic resistance genes in manure, biosolids, and fertilized soil. *J. Environ. Qual.* **2011**, *40*, 248–255. [[CrossRef](#)]
9. Wang, Q.; Wang, P.; Yang, Q. Occurrence and diversity of antibiotic resistance in untreated hospital wastewater. *Sci. Total Environ.* **2018**, *621*, 990–999. [[CrossRef](#)]
10. Lorenzo, P.; Adriana, A.; Jessica, S.; Carles, B.; Marinella, F.; Marta, L.; Luis, B.J.; Pierre, S. Antibiotic resistance in urban and hospital wastewaters and their impact on a receiving freshwater ecosystem. *Chemosphere* **2018**, *206*, 70–82. [[CrossRef](#)]
11. Zhang, M.; Meng, J.; Liu, Q.; Gu, S.; Zhao, L.; Dong, M.; Zhang, J.; Hou, H.; Guo, Z. Corn stover-derived biochar for efficient adsorption of oxytetracycline from wastewater. *J. Mater. Res.* **2019**, *34*, 3050–3060. [[CrossRef](#)]
12. Fu, H.; Li, X.; Wang, J.; Lin, P.; Chen, C.; Zhang, X.; Suffet, I.H. Activated carbon adsorption of quinolone antibiotics in water: Performance, mechanism, and modeling. *J. Environ. Sci.* **2017**, *56*, 145–152. [[CrossRef](#)] [[PubMed](#)]
13. Cuerda-Correa, E.M.; Alexandre-Franco, M.F.; Fernandez-Gonzalez, C. Advanced oxidation process for the removal of antibiotics from water. An overview. *Water* **2020**, *12*, 102. [[CrossRef](#)]
14. Liu, P.; Wu, Z.; Abramova, A.V.; Cravotto, G. Sonochemical processes for the degradation of antibiotics in aqueous solution: A review. *Ultrason. Sonochem.* **2021**, *74*, 105566. [[CrossRef](#)] [[PubMed](#)]
15. Wang, J.; Zhuan, R.; Chu, L. The occurrence, distribution and degradation of antibiotics by ionizing radiation: An overview. *Sci. Total Environ.* **2019**, *646*, 1385–1397. [[CrossRef](#)]
16. Xu, Y.; Liu, J.; Xie, M.; Jing, L.; Xu, H.; She, X.; Li, H.; Xie, J. Construction of novel CNT/LaVO₄ nanostructures for efficient antibiotic photodegradation. *Chem. Eng. J.* **2019**, *357*, 487–497. [[CrossRef](#)]
17. Iakovides, I.C.; Michael-Kordatou, I.; Moreira, N.F.F.; Ribeiro, A.R.; Fernandes, T.; Pereira, M.F.R.; Nunes, O.C.; Manaia, C.M.; Silva, A.M.T.; Fatta-Kassinos, D. Continuous ozonation of urban wastewater: Removal of antibiotics, antibiotic-resistant *Escherichia coli* and antibiotic resistance genes and phytotoxicity. *Water Res.* **2019**, *159*, 333–347. [[CrossRef](#)]
18. Guo, M.-T.; Yuan, Q.-B.; Yang, J. Distinguishing effects of ultraviolet exposure and chlorination on the horizontal transfer of antibiotic resistance genes in municipal wastewater. *Environ. Sci. Technol.* **2015**, *49*, 5771–5778. [[CrossRef](#)]
19. Lan, L.; Kong, X.; Sun, H.; Li, C.; Liu, D. High removal efficiency of antibiotic resistance genes in swine wastewater via nanofiltration and reverse osmosis processes. *J. Environ. Manag.* **2019**, *231*, 439–445. [[CrossRef](#)]
20. Li, N.; Sheng, G.-P.; Lu, Y.-Z.; Zeng, R.J.; Yu, H.-Q. Removal of antibiotic resistance genes from wastewater treatment plant effluent by coagulation. *Water Res.* **2017**, *111*, 204–212. [[CrossRef](#)]
21. Parvulescu, V.I.; Epron, F.; Garcia, H.; Granger, P. Recent progress and prospects in catalytic water treatment. *Chem. Rev.* **2022**, *122*, 2981–3121. [[CrossRef](#)] [[PubMed](#)]
22. Mathur, P.; Sanyal, D.; Callahan, D.L.; Conlan, X.A.; Pfeffer, F.M. Treatment technologies to mitigate the harmful effects of recalcitrant fluoroquinolone antibiotics on the environment and human health. *Environ. Pollut.* **2021**, *291*, 118233. [[CrossRef](#)] [[PubMed](#)]
23. Fantin, B.; Duval, X.; Massias, L.; Alavoine, L.; Chau, F.; Retout, S.; Andremont, A.; Mentre, F. Ciprofloxacin dosage and emergence of resistance in human commensal bacteria. *J. Infect. Dis.* **2009**, *200*, 390–398. [[CrossRef](#)] [[PubMed](#)]

24. Khan, G.J.; Khan, R.A.; Majeed, I.; Siddiqui, F.A.; Khan, S. Ciprofloxacin; the frequent use in poultry and its consequences on human health. *Professional Med. J.* **2015**, *22*, 001–005. [[CrossRef](#)]
25. Fasugba, O.; Gardner, A.; Mitchell, B.G.; Mnatzaganian, G. Ciprofloxacin resistance in community- and hospital-acquired *Escherichia coli* urinary tract infection: A systematic review and meta-analysis of observational studies. *BMC Infect. Dis.* **2015**, *15*, 545. [[CrossRef](#)]
26. Canada-Canada, F.; de la Peña, A.M.; Espinosa-Mansilla, A. Analysis of antibiotics in fish samples. *Anal. Bioanal. Chem.* **2009**, *395*, 987–1008. [[CrossRef](#)]
27. Zhang, Y.; Teng, Y.; Qin, Y.; Ren, Z.; Wang, Z. Determination of ciprofloxacin in fish by surface-enhanced raman scattering using a liquid-liquid self-assembled gold nanofilm. *Anal. Lett.* **2020**, *53*, 660–670. [[CrossRef](#)]
28. Jiang, W.-T.; Chang, P.-H.; Wang, Y.-S.; Tsai, Y.; Jean, J.-S.; Li, Z.; Krukowski, K. Removal of ciprofloxacin from water by birnessite. *J. Hazard. Mater.* **2013**, *250*, 362–369. [[CrossRef](#)]
29. Zaviska, F.; Drogui, P.; Grasmick, A.; Azais, A.; Heran, M. Nanofiltration membrane bioreactor for removing pharmaceutical compounds. *J. Membr. Sci.* **2013**, *429*, 121–129. [[CrossRef](#)]
30. Ye, J.-S.; Liu, J.; Ou, H.-S.; Wang, L.-L. Degradation of ciprofloxacin by 280 nm ultraviolet-activated persulfate: Degradation pathway and intermediate impact on proteome of *Escherichia coli*. *Chemosphere* **2016**, *165*, 311–319. [[CrossRef](#)]
31. Matzek, L.W.; Tipton, M.J.; Farmer, A.T.; Steen, A.D.; Carter, K.E. Understanding electrochemically activated persulfate and its application to ciprofloxacin abatement. *Environ. Sci. Technol.* **2018**, *52*, 5875–5883. [[CrossRef](#)] [[PubMed](#)]
32. Malakootian, M.; Ahmadian, M. Removal of ciprofloxacin from aqueous solution by electro-activated persulfate oxidation using aluminum electrodes. *Water Sci. Technol.* **2019**, *80*, 587–596. [[CrossRef](#)] [[PubMed](#)]
33. Bel, E.D.; Dewulf, J.; Witte, B.D.; Langenhove, H.V.; Janssen, C. Influence of pH on the sonolysis of ciprofloxacin: Biodegradability, ecotoxicity and antibiotic activity of its degradation products. *Chemosphere* **2009**, *77*, 291–295. [[CrossRef](#)] [[PubMed](#)]
34. Luo, L.; Zou, D.; Lu, D.; Xin, B.; Zhou, M.; Zhai, X.; Ma, J. Heterogeneous catalytic ozonation of ciprofloxacin in aqueous solution using a manganese-modified silicate ore. *RSC Adv.* **2018**, *8*, 33534. [[CrossRef](#)]
35. Yang, H.; Li, Y.; Chen, Y.; Ye, G.; Sun, X. Comparison of ciprofloxacin degradation in reclaimed water by UV/chlorine and UV/persulfate advanced oxidation processes. *Water Environ. Res.* **2019**, *91*, 1576–1588. [[CrossRef](#)]
36. Bobu, M.; Yediler, A.; Siminiceanu, I.; Schulte-Hostede, S. Degradation studies of ciprofloxacin on a pillared iron catalyst. *Appl. Catal. B-Environ.* **2008**, *83*, 15–23. [[CrossRef](#)]
37. Gupta, A.; Garg, A. Degradation of ciprofloxacin using Fenton's oxidation: Effect of operating parameters, identification of oxidized by-products and toxicity assessment. *Chemosphere* **2018**, *193*, 1181–1188. [[CrossRef](#)]
38. de Lima Perini, J.A.; Perez-Moya, M.; Nogueira, R.F.P. Photo-Fenton degradation kinetics of low ciprofloxacin concentration using different iron sources and pH. *J. Photochem. Photobiol. A* **2013**, *259*, 53–58. [[CrossRef](#)]
39. Diao, Z.-H.; Xu, X.-R.; Jiang, D.; Li, G.; Liu, J.-J.; Kong, L.-J.; Zuo, L.-Z. Enhanced catalytic degradation of ciprofloxacin with FeS₂/SiO₂ microspheres as heterogeneous Fenton catalyst: Kinetics, reaction pathways and mechanism. *J. Hazard. Mater.* **2017**, *327*, 108–115. [[CrossRef](#)]
40. Torniaainen, K.; Tammilehto, S.; Ulvi, V. The effect of pH, buffer type and drug concentration on the photodegradation of ciprofloxacin. *Int. J. Pharm.* **1996**, *132*, 53–61. [[CrossRef](#)]
41. El-Kemary, M.; El-Shamy, H.; El-Mehasseb, I. Photocatalytic degradation of ciprofloxacin drug in water using ZnO nanoparticles. *J. Lumin.* **2010**, *130*, 2327–2331. [[CrossRef](#)]
42. Yan, Y.; Sun, S.; Song, Y.; Yan, X.; Guan, W.; Liu, X.; Shi, W. Microwave-assisted in situ synthesis of reduced graphene oxide-BiVO₄ composite photocatalysts and their enhanced photocatalytic performance for the degradation of ciprofloxacin. *J. Hazard. Mater.* **2013**, *250*, 106–114. [[CrossRef](#)] [[PubMed](#)]
43. Gad-Allah, T.A.; Ali, M.E.M.; Badawy, M.I. Photocatalytic oxidation of ciprofloxacin under simulated sunlight. *J. Hazard. Mater.* **2011**, *186*, 751–755. [[CrossRef](#)] [[PubMed](#)]
44. Malakootian, M.; Nasiri, A.; Gharaghani, M.A. Photocatalytic degradation of ciprofloxacin antibiotic by TiO₂ nanoparticles immobilized on a glass plate. *Chem. Eng. Commun.* **2020**, *207*, 56–72. [[CrossRef](#)]
45. Kaur, A.; Anderson, W.A.; Tanvir, S.; Kansal, S.K. Solar light active silver/iron oxide/zinc oxide heterostructure for photodegradation of ciprofloxacin, transformation products and antibacterial activity. *J. Colloid Interface Sci.* **2019**, *557*, 236–253. [[CrossRef](#)]
46. Lee, Y.; Lee, W. Degradation of trichloroethylene by Fe(II) chelated with cross-linked chitosan in a modified Fenton reaction. *J. Hazard. Mater.* **2010**, *178*, 187–193. [[CrossRef](#)]
47. Marques Neto, J.d.O.; Bellato, C.R.; Milagres, J.L.; Pessoa, K.D.; de Alvarenga, E.S. Preparation and evaluation of chitosan beads immobilized with Iron(III) for the removal of As(III) and As(V) from water. *J. Braz. Chem. Soc.* **2013**, *24*, 121–132. [[CrossRef](#)]
48. Trung, T.S.; Thein-Han, W.W.; Qui, N.T.; Ng, C.-H.; Stevens, W.F. Functional characteristics of shrimp chitosan and its membranes as affected by the degree of deacetylation. *Bioresour. Technol.* **2006**, *97*, 659–663. [[CrossRef](#)]
49. Queiroz, M.F.; Melo, K.R.T.; Sabry, D.A.; Sassaki, G.L.; Rocha, H.A.O. Does the use of chitosan contribute to oxalate kidney stone formation? *Mar. Drugs* **2015**, *13*, 141–158. [[CrossRef](#)]
50. Hernandez, R.B.; Franco, A.P.; Yola, O.R.; Lopez-Delgado, A.; Felcman, J.; Recio, M.A.L.; Merce, A.L.R. Coordination study of chitosan and Fe³⁺. *J. Mol. Struct.* **2008**, *877*, 89–99. [[CrossRef](#)]

51. Gütlich, P. Fifty Years of Mossbauer Spectroscopy in Solid State Research—Remarkable Achievements, Future Perspectives. *Z. Anorg. Allg. Chem.* **2012**, *638*, 15–43. [[CrossRef](#)]
52. Chiessi, E.; Paradossi, G.; Venanzi, M.; Pispisa, B. Association complexes between Fe(III) or Cu(II) ions and chitosan derivatives. A thermodynamic and spectroscopic investigation. *Int. J. Biol. Macromol.* **1993**, *15*, 145–151. [[CrossRef](#)]
53. Bhatia, S.C.; Ravi, N. A magnetic study of a Fe-chitosan complex and its relevance to other biomolecules. *Biomacromolecules* **2000**, *1*, 413–417. [[CrossRef](#)] [[PubMed](#)]
54. Webster, A.; Halling, M.D.; Grant, D.M. Metal complexation of chitosan and its glutaraldehyde cross-linked derivative. *Carbohydr. Res.* **2007**, *342*, 1189–1201. [[CrossRef](#)] [[PubMed](#)]
55. Zhu, H.-Y.; Xiao, L.; Jiang, R.; Zeng, G.-M.; Liu, L. Efficient decolorization of azo dye solution by visible light-induced photocatalytic process using SnO₂/ZnO heterojunction immobilized in chitosan matrix. *Chem. Eng. J.* **2011**, *172*, 746–753. [[CrossRef](#)]
56. Saha, T.K.; Ichikawa, H.; Fukumori, Y. Gadolinium diethylenetriaminopentaacetic acid-loaded chitosan microspheres for gadolinium neutron-capture therapy. *Carbohydr. Res.* **2006**, *341*, 2835–2841. [[CrossRef](#)]
57. Katsumata, H.; Kaneco, S.; Suzuki, T.; Ohta, K.; Yobiko, Y. Photo-Fenton degradation of alachlor in the presence of citrate solution. *J. Photochem. Photobiol. A* **2006**, *180*, 38–45. [[CrossRef](#)]
58. Feng, J.; Hu, X.; Yue, P.L.; Zhu, H.Y.; Lu, G.Q. Degradation of Azo-dye orange II by a photoassisted Fenton reaction using a novel composite of iron oxide and silicate nanoparticles as a catalyst. *Ind. Eng. Chem. Res.* **2003**, *42*, 2058–2066. [[CrossRef](#)]
59. Feng, J.; Hu, X.; Yue, P.L.; Zhu, H.Y.; Lu, G.Q. Discoloration and mineralization of reactive red HE-3B by heterogeneous photo-Fenton reaction. *Water Res.* **2003**, *37*, 3776–3784. [[CrossRef](#)]
60. Sum, O.S.N.; Feng, J.; Hu, X.; Yue, P.L. Pillared laponite clay-based Fe nanocomposites as heterogeneous catalysts for photo-Fenton degradation of acid black 1. *Chem. Eng. Sci.* **2004**, *59*, 5269–5275.
61. Tamimi, M.; Qoural, S.; Barka, N.; Assabbane, A.; Ait-Ichou, Y. Methomyl degradation in aqueous solutions by Fenton's reagent and the photo-Fenton system. *Sep. Purif. Technol.* **2008**, *61*, 103–108. [[CrossRef](#)]
62. Pouretedal, H.R.; Kadkhodaie, A. Synthetic CeO₂ nanoparticle catalysis of methylene blue photodegradation: Kinetics and mechanism. *Chin. J. Catal.* **2010**, *31*, 1328–1334. [[CrossRef](#)]
63. Desesso, J.M.; Scialli, A.R.; Goeringer, G.C. D-Mannitol, a specific hydroxyl free radical scavenger, reduces the developmental toxicity of hydroxyurea in rabbits. *Teratology* **1994**, *49*, 248–259. [[CrossRef](#)] [[PubMed](#)]
64. Bill, E. *Mfit*; Max-Planck Institute for Chemical Energy Conversion: Mülheim/Ruhr, Germany, 2008.
65. Saha, T.K.; Frauendorf, H.; John, M.; Dechert, S.; Meyer, F. Efficient oxidative degradation of azo dyes by a water-soluble manganese porphyrin catalyst. *ChemCatChem* **2013**, *5*, 796–805. [[CrossRef](#)]
66. Sarker, S.R.; Polash, S.A.; Boath, J.; Kandjani, A.E.; Poddar, A.; Dekiwadia, C.; Shukla, R.; Sabri, Y.; Bhargava, S.K. Functionalization of elongated tetrahedral Au nanoparticles and their antimicrobial activity assay. *ACS Appl. Mater. Interfaces* **2019**, *11*, 13450–13459. [[CrossRef](#)]